Journal of Cleaner Production 425 (2023) 138664

Contents lists available at ScienceDirect

Journal of Cleaner Production

journal homepage: www.elsevier.com/locate/jclepro

Simulation and multi-objective assessment of an environmentally friendly trigeneration system powered by biogas from landfilling using a novel cascade heat integration model

Wu Shao [a,***], Ayman A. Ghfar [b], Aliashim Albani [c,**], Manoj Kumar Agrawal [d], Fahid Riaz [e], Kwanho Shi [f,*]

[a] Shaoyang University, Daxiang District, Shaoyang City, Hunan Province, 422000, China
[b] Department of Chemistry, College of Science, King Saud University, P.O. Bo x 2455, Riyadh, 11451, Saudi Arabia
[c] Faculty of Ocean Engineering Technology and Informatics, Universiti Malaysia Terengganu, 21030, Kuala Nerus, Terengganu, Malaysia
[d] GLA University, Mathura, UP, 281406, India
[e] College of Engineering, Abu Dhabi University, Abu Dhabi, United Arab Emirates
[f] Sustainable Management of Natural Resources and Environment Research Group, Faculty of Environment and Labour Safety, Ton Duc Thang University, Ho Chi Minh City, Viet Nam

ARTICLE INFO

Handling Editor: Panos Seferlis

Keywords:
Trigeneration process
Cascade heat recovery
Landfill biogas fuel
Eco-friendly design
Economic analysis
Carbon dioxide footprint

ABSTRACT

This study introduces a novel integrated trigeneration system fed by biogas fuel from landfilling, promoting environmentally sustainable practices. In the system proposed within this study, fuel combustion occurs through the implementation of a gas turbine cycle, while the subsequent waste heat is efficiently recuperated within a cascade framework. The combustion process is combined with a supercritical carbon dioxide cycle, an organic Rankine cycle, an ammonia Rankine cycle, a seawater desalination unit, and a Kalina cycle. The process is simulated using the Aspen HYSYS software while conducting a comprehensive analysis encompassing the energy, exergy, economic, and environmental aspects. In view of the thermodynamic perspective, the analysis yields values of 70.28%, 24.89%, and 57.51% for the energy utilization factor, and thermal and exergy efficiencies, respectively. The subsequent environmental results illustrate that the proposed scheme exhibits a carbon dioxide emission level of 0.272 $kgCO_2/kWh$, yielding a noteworthy reduction of 51.02% in carbon dioxide emissions compared to a traditional power and heat generation system. Besides, the economic analysis demonstrates a positive net present value of 779, 571, 045 $ for the proposed process. Furthermore, the total unit cost of products and cost of energy are found at 12.25 $/GJ and 0.022 $/kWh, respectively.

1. Introduction

Given the exhaustion of fossil fuel and hydrocarbon reserves, it is imperative to deliberate on the utilization of alternate fuel or energy sources (Cheng et al., 2023; Guedri et al., 2023; Wang et al., 2022). This technique, in combination with diverse production techniques, can address the energy crisis in the future (Jiang et al., 2022). Biogas power plants (BPPs) are known as one of the most important alternatives for conventional plants that can produce power and heat utilizing organic waste as input fuel sources (Wang et al., 2023). The procedure involves aggregating biodegradable substances, including manure, food scraps, and wastewater, which are introduced into an anaerobic digester. Within this system, microorganisms facilitate the decomposition of these materials, resulting in biogas generation (Yu et al., 2023). The biomass can subsequently be harnessed to generate thermal energy or electrical power using combustion engines and turbines (Han et al., 2023). The heat produced can be used for water heating or generating thermal energy, while the power can be used on-site or sold to the power grid (Atelge et al., 2021). This ability has been evaluated in previous studies, some of which are reviewed in the following.

Zhao et al. (2023) presented an innovative polygeneration process that used biogas to produce potable water, CO_2, methanol, and heat. The model was examined from the environmental, energy, economic, and

* Corresponding author.
** Corresponding author.
*** Corresponding author.
E-mail addresses: swsyxy@126.com (W. Shao), a.albani@umt.edu.my (A. Albani), kwanhoshi58@gmail.com (K. Shi).

https://doi.org/10.1016/j.jclepro.2023.138664
Received 5 June 2023; Received in revised form 23 August 2023; Accepted 3 September 2023
Available online 8 September 2023

Nomenclature

A	Area
e	Specific exergy
e_i^{ch}	Standard molar chemical exergy
$\dot{E}_D$	Exergy destruction
$\dot{E}$	Exergy rate
F	Molar flow rate
h	Specific enthalpy
i	Annual interest rate
LHV	Lower heating value
n	Lifetime of the system
$\dot{m}$	Mass flow rate
P	Pressure
$\dot{Q}$	Thermal energy rate
R	Universal gas constant
s	Specific entropy
t_y	Annual working hours for plant
T	Temperature
U	Overall heat loss coefficient
v	Molar volume
$\dot{W}$	Power

Greek symbols

$\beta_{net}^{CO_2}$	Total CO_2 emission
η	Isentropic efficiency
λ_{el}	Electrical efficiency
λ_{th}	Thermal efficiency
μ	Emission factor
φ_{ex}	Exergy efficiency
ξ_{CO_2}	Total indirect emissions
ϑ_{CO_2}	Total direct emission
Ψ_{CO_2}	Intensity of CO_2 emission

Subscripts and Superscripts

0	Reference state
CH	Chemical
F	Fuel
in	Input
out	Output
P	Product
PH	Physical
tri	Trigeneration

Abbreviations

ARC	Ammonia Rankine cycle
BPP	Biogas power plant
CCHP	Combined cooling, heat, and power
CHP	Combined heat and power
COE	Cot of energy
FCI	Fixed capital investment
GHG	Greenhouse gas
LNG	Liquefied natural gas
NPV	Net present value
ORC	Organic Rankine cycle
PES	Primary energy savings
PRSV	Peng–Robinson-Stryjek-Vera
SPU	Supercritical power unit
SWDS	Seawater desalination section
TAC	Total annual cost
TCI	Total cost investment
TPC	Total product cost
TUCP	Total unit cost of product
WHR	Waste hear recovery

exergy perspectives, showing low CO_2 emission intensity and high exergetic and energetic efficiencies. Methane content of biogas was increased through chemical absorption, improving the overall efficiency and reducing production costs. Hai et al. (2023) suggested a process to produce methanol, desalinated water, and oxygen with negative CO_2 emissions and lower costs using landfill gas upgrading. The process included nine subsystems with high energy and exergy efficiencies, and increasing the H_2/CO_2 ratio improved carbon and energy efficiency while decreasing CO_2 emissions. He et al. (2023) evaluated an integrated system that produced cooling load, electricity, and hydrogen using biomass. Purification and steam reforming processes were combined to increase the efficiency of hydrogen production with exergetic and energetic efficiencies of about 31.14% and 31.51%, respectively. Siddiqui and Dincer (2021) developed an energy system that used rice husk biomass to generate power and produce multiple useful commodities while recovering waste heat. The system also included a water treatment process that produced freshwater from wastewater brine with 69.4% as an energetic efficiency. Behzadi et al. (2020) evaluated a biomass-fired system utilizing steam as the agent for gasification for power and heat production, while minimizing the content of biogas moisture to achieve high efficiency and low costs. Hashemian and Noorpoor (2019) examined a multigeneration scheme relying on biomass fuel and solar energy that generated electric power, hydrogen, heating, potable water, and coolant. The system's feasibility, environmental impact, and optimization were analyzed using thermodynamic analysis, exergoeconomic modeling, and optimization techniques. Safari and Dincer (2019) proposed a multigeneration system to generate power, potable water, hydrogen, and heat using biogas as fuel. Power plant waste heat was utilized for desalination and heating while excess electricity generation was utilized for electrochemical hydrogen production. dos Santos et al. (2018) explored the utilization of renewable biogas resources as an alternative feedstock for methanol production. The study used mathematical modeling and simulation to compare four different biogas sources for methanol production and found that palm oil effluent was the most profitable source while landfill gas had limited capacity.

Waste heat recovery technology (WHR) has become a popular solution in various industries to reduce energy consumption and their carbon footprint. It has been implemented successfully in power plants, chemical plants, and other manufacturing facilities. The recovered waste heat is able to be employed for providing heating for buildings or industrial processes, generate electricity, or drive turbines. In addition to reducing greenhouse gas emissions, WHR can also improve the total operational system efficiency and reduce dependence on fossil fuels. By integrating WHR into multigeneration systems, companies can enhance their environmental sustainability and achieve significant cost savings over time (Chen et al., 2022). Gu et al. (2023) described a co-generation process that produced methanol by capturing CO_2 from power system and using an alkaline reactor to supply hydrogen. A wasted heat recovery scheme with the environmental, energetic, financial, and exergy perspectives employed to evaluate the process efficiency. The total exergetic and energetic efficiencies achieved were about 76% and 64.13%, respectively. Zhang et al. (2023) evaluated using an organic Rankine cycle (ORC) to regain heat in natural gas liquefaction. The study illustrated that using an ORC cycle enhanced exergy efficiency, reduced power consumption, and lowered CO_2 emissions. A modified ORC increased total exergy efficiency by 10.2% and reduced power consumption by around 19%. Tian et al. (2023) proposed a scheme to generate electricity and potable water through cogeneration utilizing waste heat recovery from natural gas integrated power plant, with an efficiency of 74%. Using flue gas as the feed, the system produced 892.4 MWh of power and 6656.8 m^3 of potable water annually at a total annual cost of 1,559,491.11 $ and 598,833.11 $/year as the return on investment. Arslan and Yılmaz (2022) discussed using biomass as renewable energy and integrating ORC to regain waste heat in an Afyon biogas system. The outcomes demonstrated a growth in net power production and performance. The study emphasized the importance of waste heat recovery for optimizing biomass-based power plant performance. Dai et al. (2009) focused on the use of ORC with various working fluids to regain low-grade waste heat. The research found that organic working fluids were more efficient at converting waste heat to useful work. R236EA had the maximum exergetic efficiency, and adding an internal heat exchanger did not improve ORC performance under given conditions.

Combined heat and power (CHP) plants are well-organized plants that yield both heat-based energy and electricity from a single fuel resource. The process involves the generation of electricity and heat, such as hot water or steam, in a single, integrated system. This high level of efficiency can lead to considerable cost savings, decreased greenhouse gas emissions, and improved energy security. Therefore, CHP systems offer a sustainable and efficient energy solution that benefits both the environment and the economy (Erixno et al., 2022). Regarding this, Liu et al. (2023) suggested a new system that combined geothermal energy, an electrolyzer, and an oxyfuel combustion power plant for efficient production of multiple products. A thorough analysis is conducted on various aspects such as energy, exergy, environment, and economics through a parametric study, which demonstrates the effectiveness of this approach with minimal carbon footprint. Cao et al. (2022) evaluated the development of an integrated heat and power plants that utilized a carbon dioxide (CO_2) Brayton cycle and a fuel cell. The study analyzed parameters including equivalence ratio, fuel utilization factor, and fuel cell temperature to determine their effects on power and heat production. The research provided regression models and optimal conditions for achieving maximum power and heat. Fang et al. (2021) proposed an integrated electricity, heating, and cooling system that used the waste heat of the exhaust gas and cold of the energy liquified natural gas. The system achieved high efficiencies and low costs, as demonstrated through thermodynamic and exergoeconomic analyses and single and multi-objective optimizations. Mohammadi et al. (2018) analyzed a combination of heat and power plant to recover maximum heat from exhaust gases. The optimization of product cost rate and exergetic efficiency was done through multi-objective optimization with seven different decision parameters. The results demonstrated that steam turbine back pressure and inlet pressure led to the maximum effect on the exergetic efficiency and product cost rate. A combination of coolant, heat and power (CCHP) arrangement consisted of a molten carbonate fuel cell as its primary power source, a Stirling engine, and an absorption chiller was introduced by Mehrpooya et al. (2017). The system provided significant power output along with heat and cold duty, making it an efficient solution for CHP applications.

The assessment of greenhouse gas emissions is crucial in determining the environmental impact and identifying areas for reduction in multigeneration systems. Analyzing these emissions can lead to economic benefits through efficiency improvements, while also demonstrating a commitment to sustainability and corporate social responsibility. Gas emission assessment plays a critical role in promoting sustainable energy production and reducing the negative impact of human activities on the environment (Salimi et al., 2022). Xiao et al. (2023) introduced a system that combined methanol production, liquefied natural gas, and crude helium was highly efficient with regard to energy and exergy. Moreover, the environmental analysis illustrated that the majority of CO_2 emissions were indirect, and the economic analysis estimated the total annual cost and net present value of the proposed structure. Elsayed et al. (2021) designed multigeneration system utilized waste heat to drive various cycles. The results depicted a 34.2% reduction in energy consumption and a 39.3% reduction in CO_2 emissions made a comparison of stand-alone systems for potable water, electricity, and cooling production. Chahartaghi and Sheykhi (2018) perused a trigeneration system that reduced fuel consumption and pollutant emission by using different cycles. The study investigated the impacts of heater wall temperature, engine rotational speed, regenerator length, CO_2 emissions reduction, and fuel consumption. The results indicated a reduction of 31.83% in fuel consumption and 38.44% in CO_2 emission compared to common energy plants. A novel approach called ***trigeneration CO_2 emission reduction*** (TCO_2ER) was evaluated by Chicco and Mancarella (2008a) to evaluate the CO_2 reduction and other greenhouse gas emissions from CCHP and CHP plants. The effectiveness of this approach was demonstrated for various trigeneration and cogeneration plants. Chicco and Mancarella (2008b) provided particular examples to demonstrate the efficacy of TCO_2ER indicator in evaluating greenhouse gas (GHG) emission reduction from plants. The paper evaluates various emission indicators for multigeneration plants with various of equipment and carries out scenario analyses to examine emission reduction advantages in regions with different energy generation frameworks.

Based on the literature review conducted, it can be inferred that the employment of biomass-biogas-based multigeneration configurations presents a viable solution for sustainable production, marked by commendable thermodynamic, economic, and environmental performances. However, further investigation is required to determine the optimal means of waste heat recovery in order to effectively reduce the emission of CO_2 and enhance the overall efficiency of the configurations under consideration. In this regard, the main innovations corresponding to the proposed study are summarized as follows:

- Limited research has been undertaken to demonstrate the viability of utilizing biogas fuel derived from landfilling for multigeneration purposes. Therefore, the present study introduces and assesses an innovative multigeneration system utilizing this approach for the first time.
- This study presents a development of an effective cascade heat integration strategy within the framework of a biogas-fired power plant. The primary objective of this integration is to diminish the level of thermodynamic irreversibility, thereby enhancing the overall exergy efficiency in comparison to prior investigations. This study incorporates a supercritical power unit, a Kalina cycle, an ORC/ARC power plant, and a seawater desalination unit.
- Primary energy savings (PES) by reducing the consumption of primary energy when producing power and heat separately (product separation) compared to other studies.
- The devised system presents an environmentally friendly method featuring reduced CO_2 emission in contrast to preceding research endeavors to generate electricity, heating, and fresh water simultaneously.

The computational emulation of this system has been executed via the Aspen HYSYS software, followed by a comprehensive evaluation encompassing the four domains of energy, exergy, economy, environment (4E). Furthermore, a sensitivity parametric analysis is carried out to illustrate the fluctuation of primary performance indicators in response to the operating parameters of the system.

2. Process description

Fig. 1 presents the overall schematic of the integrated trigeneration process. This new structure designed based on cascade heat integration method is essentially a CHP system that utilizes thermal integration through water desalination. Cascade heat integration is widely recognized as a highly efficient approach for heat recovery and generating additional products. In accordance with this method, the enthalpy level of the energetic waste stream is aligned with the subsequent subsystem,

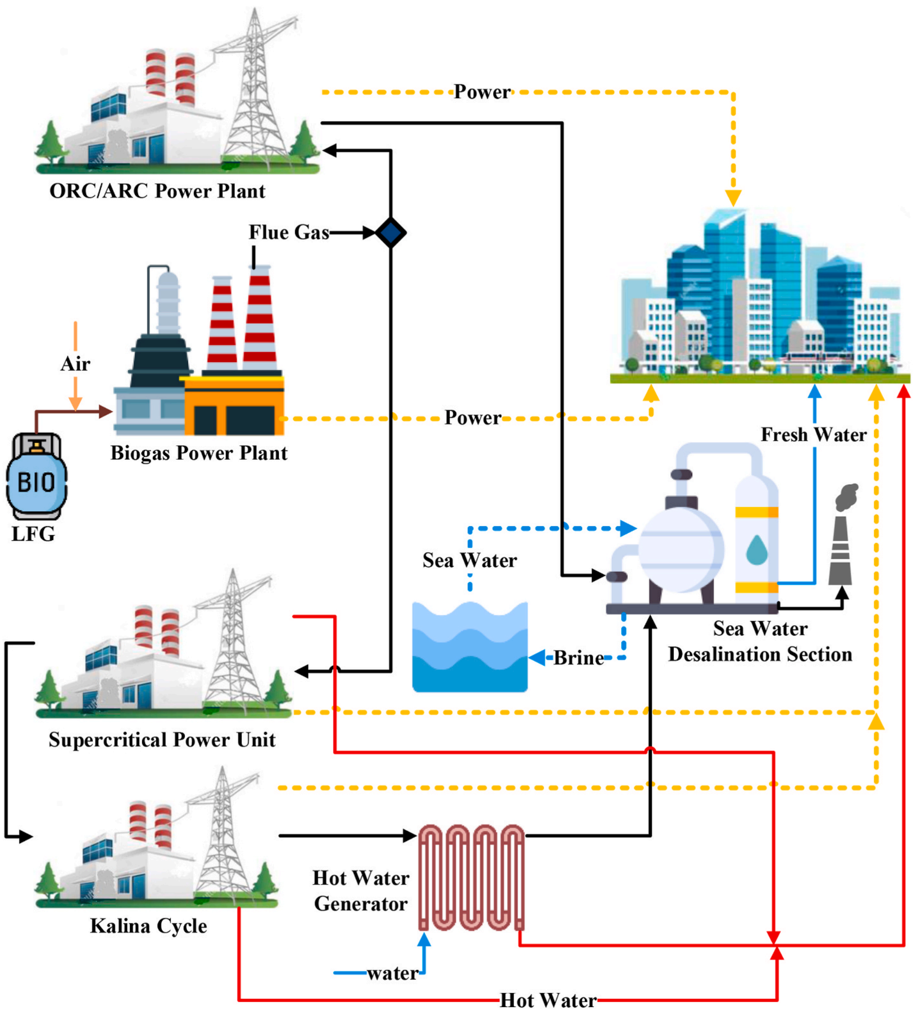

Fig. 1. Schematic diagram for the proposed Trigeneration process.

thereby sequentially facilitating heat recovery. In addition, the proposed process has an extensive heat exchange network for recovering waste heat in all subsystems, which results in maximum fuel efficiency for LF biogas. The only source of energy for this new process is biogas produced from waste disposal, which generates a significant amount of energy upon combustion in the chamber and is made available to other subsystems.

This proposed structure consists of sections such as the BPP, supercritical power unit (SPU), Kalina cycle, ORC/ARC power plant (OAPP), and seawater desalination section (SWDS). Fuel combustion in the BPP produces a large amount of energy that supplies all the electricity needed in the process, and the excess electricity generated in other subsystems can be used for domestic or industrial purposes. The flue gas, which contains a significant amount of energy, acts as the driving force in the subsystems. In addition, to achieve higher heat integration, a fluid with a high critical temperature (octane) is employed in the OAPP section, and as a result, the excess heat of the turbine is also utilized in the ammonia Rankine cycle (ARC). Another example of heat integration in the proposed structure is the use of flue gas temperature, which decreases after heat exchange in different sections and is used for partial condensation (reducing cold utility) of the fresh water steam flow in the SWDS subsystem. Additionally, in the KC section, a heat recovery exchanger is used to condense the working fluid for hot water production (in common systems, this is done via cooling water, and no product is produced in this way). In other words, by adding a heat recovery heat exchanger to the Kalina cycle, instead of generating a single power product, this cycle simultaneously generates two products of heat and power.

Therefore, the applications of heat integration in new structures include the following:

- Using a seawater desalination system and recovering waste heat from flue gas.
- Using a heat recovery exchanger to produce hot water from waste heat from flue gas.
- Using waste heat in the KC cycle and producing hot water.
- Using the flue gas temperature for condensing water vapor under the SWDS subsystem and reducing cold utility.

Also, the potential enhancements in operational processes, aiming at achieving cleaner and sustainable production framework, can be identified as follows:

- The proposed system demonstrates a noteworthy impact in mitigating methane utilization and CO_2 emissions by utilizing a biogas fuel available from landfill resources.
- The proposed system exhibits several notable advantages concerning low irreversibility, per the principles outlined by the second law of thermodynamics. Furthermore, comparing this work's energy and exergy efficiencies with previous studies suggests that the designed system exhibits superior performance, leading to higher sustainability.

2.1. Biogas power plant

In this section, landfill biogas (stream 1) is mixed with air and supplied to the combustor. The air (stream 2) is first compressed by the K-100 compressor before entering the combustor (CRV-100), and then preheated by the E-100 heat exchanger (stream 4). Hot air passes through the T-100 turbine, expanding and generating power. The required increase in air temperature for combustion is achieved through the hot gas exiting the combustion chamber (stream 7). After heat exchange with the combustion air (stream 9), the hot gas splits into two parts and is sent to the desired subsystems as a driving force. This subsystem diagram can be seen in Fig. 2.

2.2. Supercritical power unit

According to Fig. 2, stream 11, which is a part of the hot flue gas, evaporates supercritical CO_2 working fluid in the E-101 heat exchanger (stream 13). After reaching the desired conditions, the fluid enters the T-101 turbine, where its expansion generates power. The turbine output (stream 15), by passing through the E-102 to E-104 heat exchangers, is cooled to a lower temperature and is then compressed to a higher pressure that can be sent back to the E-101 heat exchanger (stream 21) via the compressor. The K-101 compressor output has reached a higher temperature before the evaporator (stream 23) through heat exchange with the hot output fluid from the turbine, which also increases power generation. In this cycle, hot water is produced as a result of energy integration through the E-104 heat exchanger (stream 20).

2.3. Kalina cycle

The flue gas outlet from the SPU subsystem (stream 12) evaporates the working fluid, which is a mixture of water and ammonia (stream 25), in the E-105 heat exchanger and generates power by expanding steam in the T-102 turbine. The turbine output enters the S-100 separator as a two-phase flow, and the separated steam (stream 28) is expanded again by the T-103 turbine. The liquid taken from the S-100 separator passes through the E-106 recuperator, and after its pressure becomes equal to the outlet fluid pressure of the T-103 turbine at the VLV-100 expansion valve, it is mixed in this flow. The resulting mixture (stream 33) has a suitable temperature for producing hot water, and for this purpose, heat recovery and fluid condensation are also used in the E-107 heat exchanger (stream 34). The working fluid reaches the evaporator pressure again through the P-100 pump and, after passing through the recuperator and preheating, enters the Kalina cycle evaporator.

2.4. ORC/ARC power plant

The hot flue gas from the BPP subsystem (stream 10) is the driving force for the OAPP subsystem, and for this purpose, it is used in the E-109 heat exchanger to evaporate the octane working fluid (stream 43). Octane enters the T-104 expansion turbine in the vapor phase and at high pressure, where the working fluid expands and power is generated.

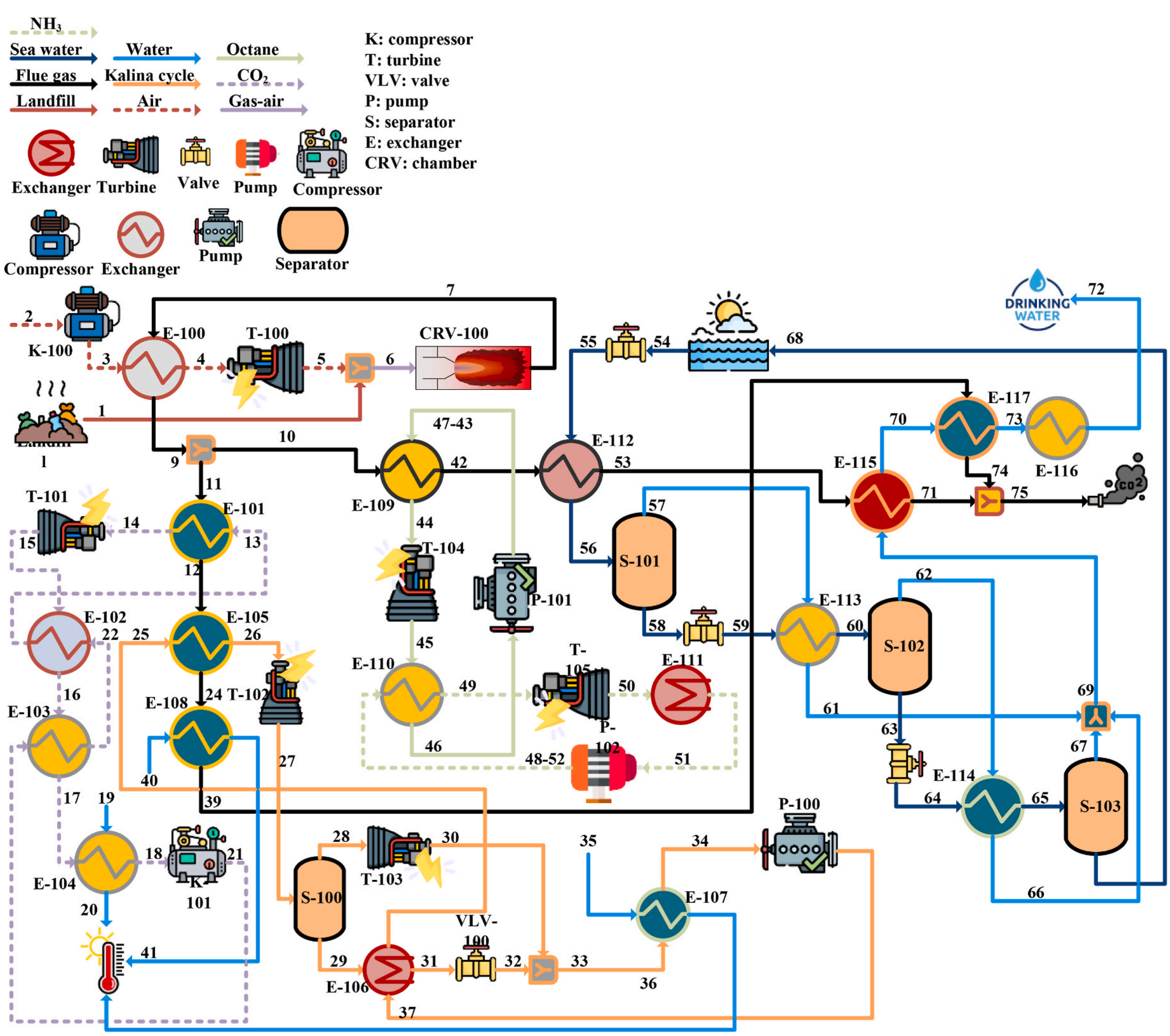

Fig. 2. Process flow diagram for proposed process.

The turbine output has a desirable temperature for heat recovery, so this temperature is used as the driving force in an ARC. Stream 45 evaporates the ammonia in the E-110 heat exchanger, and the thermal energy is converted into electrical power in the T-105 turbine. Ammonia becomes completely liquid again after expansion (stream 50) through the E-111 heat exchanger, and is re-entered into the Rankine cycle through the P-102 pump. Essentially, the ARC is a condenser for the ORC with the octane working fluid, whose main task is to recover waste heat. Finally, the octane fluid (stream 46) in the liquid phase is directed towards the evaporative heat exchanger through the P-101 pump at a pressure of 2000 kPa. The process flowchart for this cycle is also shown in Fig. 2.

2.5. Seawater desalination section

The flue gas enters the E-108 heat exchanger (stream 24) and produces hot water (stream 41) after exchanging heat with the working fluid. Next, stream 39 is sent to the E-117 heat exchanger for partial condensation of fresh water vapor (stream 70) (Fig. 2). The main driving force for seawater evaporation (stream 55) is the flue gas from the E-109 heat exchanger, which evaporates seawater in the E-112 heat exchanger. Seawater evaporates in three stages at 25, 15, and 10 kPa pressures. The operation of each effect is such that seawater enters the evaporator after pressure reduction, which consists of E-112 to E-114 heat exchangers, and after each evaporator, S-101 to S-103 separator units are used to separate fresh water vapor. Finally, the steam streams (61, 66, and 67) are collected in a mixer (stream 69), and condensation takes place in the E-116 to E-117 heat exchangers, resulting in fresh water production from the E-116 heat exchanger (stream 72).

3. Simulation of the process

Fig. 3 shows the complete simulation diagram of the proposed process. This process is numerically modeled using Aspen HYSYS Version 10, which is a specialized tool with high computing power and speed. Recently, many papers have been published on the modeling of multi-generational systems using this software, and it seems that an emerging generation of studies on multi-generational systems is being developed utilizing Aspen HYSYS (Zhao et al., 2023; Gu et al., 2023; Liu et al., 2023; Xiao et al., 2023).

Peng-Robinson's state equation has been recommended previously for simulating power and heat generation systems (Zhang et al., 2023; Tian et al., 2023). The formulation of Peng-Robinson's state equation is given below (Luján et al., 2012):

$$P = \frac{RT}{v - \frac{0.07780R\frac{T}{T_r}}{\frac{P}{P_r}}} - \frac{\frac{0.452724R^2\left(\frac{T}{T_r}\right)^2}{\frac{P}{P_r}}}{v^2 + 2bv - b^2} \tag{1}$$

In Eq. (1), P is pressure, T represents temperature, and v is molar volume, and the terms $\frac{0.452724R^2\left(\frac{T}{T_r}\right)^2}{\frac{P}{P_r}}$ and $\frac{0.07780R\frac{T}{T_r}}{\frac{P}{P_r}}$ are respectively equivalent to constants a and b in the state equation. Additionally, $\frac{T}{T_r}$ and $\frac{P}{P_r}$ represent critical temperature and critical pressure, respectively (Peng and Robinson, 1976). The simulation assumes the following:

- The system is in a steady state (Liu et al., 2023).
- Heat losses in heat exchangers are negligible (Liu et al., 2023).
- Biogas impurities are ignored.
- Kinetic and potential energies are negligible (Ji-chao and Sobhani, 2021).
- All pumps, turbines, and compressors operate under a specific isentropic efficiency (Ji-chao and Sobhani, 2021).

In Tables 1–3, the most critical input information for simulation, thermodynamic conditions (temperature, pressure, and flow rate) for the entire process streams, and the percentage composition of the main flowsheet points are listed, respectively (see Table 4).

3.1. Validation of model

In this part of the study, validation of simulation results is performed, and the results of the Aspen HYSYS flowsheet (Fig. 3) are compared with reference papers (Ji-chao and Sobhani, 2021; Ahmadi et al., 2013). Tables 5–8 report comparison results for the gas turbine subsystem, Kalina cycle, supercritical CO_2 cycle, and ORC. There is a high correlation between the Aspen HYSYS results and the reported values in papers (Ji-chao and Sobhani, 2021; Ahmadi et al., 2013), indicating the high accuracy of the Peng-Robinson state equation and the information entered into the software for convergence, according to Table 1.

Based on the findings presented in Table 5, it is evident that the gas turbine cycle analysis conducted in this study exhibits a maximum relative error of 3.64% in comparison to the corresponding results obtained by Ji-chao and Sobhani (2021). Table 6 shows the highest relative

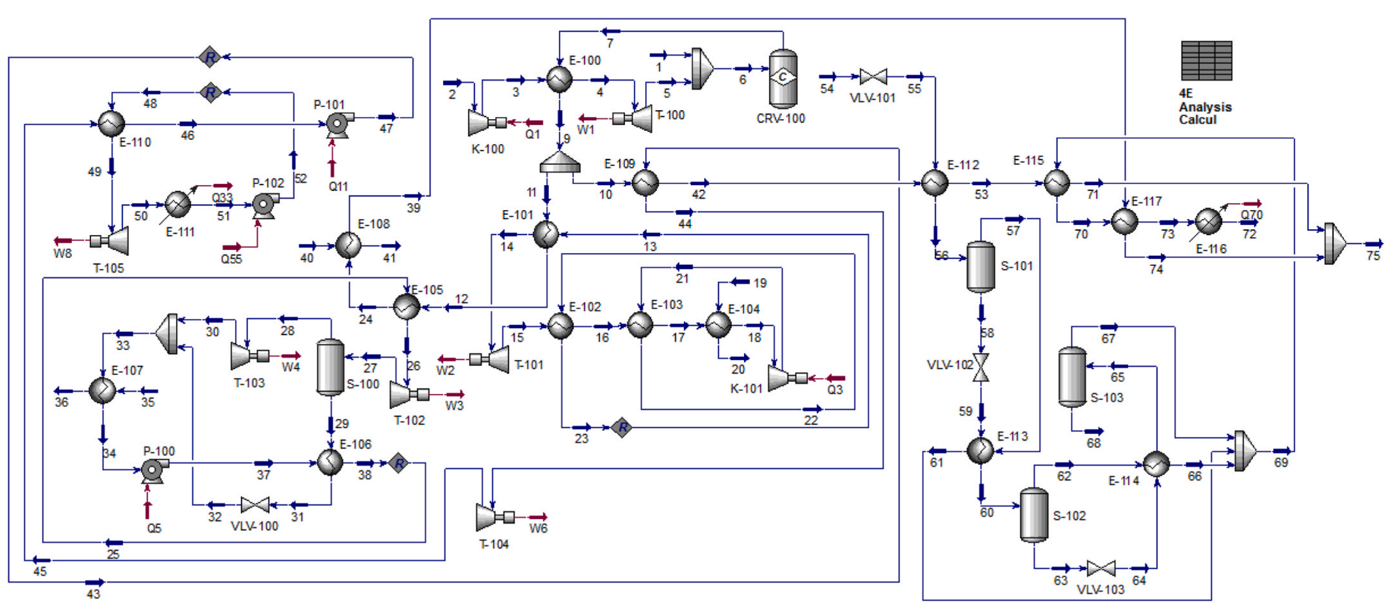

Fig. 3. Schema of the proposed process simulation.

Table 1
Parameter values for proposed process simulation.

Biogas Power Plant	
Air inlet temperature (°*C*) (Ji-chao and Sobhani, 2021)	25
Landfill Gas Composition (dos Santos et al., 2018)	Mole %
CO_2	50
CH_4	35
N_2	15
T-100 outlet pressure (kPa) (Ji-chao and Sobhani, 2021)	101
K-100 outlet pressure (kPa) (Ji-chao and Sobhani, 2021)	1418
Air temperature from E-100 (°*C*) (Ji-chao and Sobhani, 2021)	1124.1
Supercritical Power Unit (Ji-chao and Sobhani, 2021)	
Working fluid	CO_2
T-101 outlet pressure (kPa)	7500
T-101 Inlet pressure (kPa)	37,500
K-101 outlet pressure (kPa)	37,500
K-101 Inlet pressure (kPa)	7500
Ho t water temperature (°*C*)	55
Kalina Cycle (Ji-chao and Sobhani, 2021)	
Working fluid	NH_3–H_2O
T-102 outlet pressure (kPa)	2000
T-102 Inlet pressure (kPa)	20,000
T-103 outlet pressure (kPa)	247
T-103 Inlet pressure (kPa)	2000
Ho t water temperature (°*C*)	55
P-100 outlet pressure (kPa)	20,000
P-100 Inlet pressure (kPa)	2000
VLV-100 outlet pressure (kPa)	247
Organic Rankine Cycle (High Temperature) (Ahmadi et al., 2013)	
Working fluid	n-octane
T-104 outlet pressure (kPa)	28.09
T-104 Inlet pressure (kPa)	2000
P-101 outlet pressure (kPa)	2000
P-101 Inlet pressure (kPa)	28.09
E-109 pressure drop (kPa)	0.0
Octane temperature from E-109 (°*C*)	400
Rankine Cycle (Low Temperature) (Dai et al., 2009)	
Working fluid	NH3
T-105 outlet pressure (kPa)	1003
T-105 Inlet pressure (kPa)	3900
P-102 outlet pressure (kPa)	3900
P-102 Inlet pressure (kPa)	1003
Sea Water Desalination Section	
Sea water inlet pressure (kPa) (Ghorbani et al., 2020)	101.3
Sea water inlet temperature (°*C*) (Ghorbani et al., 2020)	25
Sea water flow rate (kg/s)	25.72
S-101 operating pressure (kPa)	25
S-102 operating pressure (kPa)	15
S-103 operating pressure (kPa)	10
E-116 temperature (°*C*)	35

error observed for the supercritical CO_2 cycle compared to Ji-chao and Sobhani (2021) is 6.55%. Table 7 shows that the Kalian cycle has the highest relative error of 2.68% compared to Ji-chao and Sobhani (2021). According to the data presented in Table 8, a comparison is conducted between the compositional aspects of the current study and the study conducted by Ahmadi et al. (2013). This comparison demonstrates the highest relative error of 2.01%.

4. Analysis of the process

4.1. Energy analysis

Energy analysis is of utmost significance as it facilitates a thorough comprehension of energy systems and their consumption/production patterns (Cheng et al., 2021). Through the implementation of energy analysis, it is possible to evaluate the effectiveness and long-term viability of different energy sources and systems (Haghghi et al., 2023). Moreover, energy analysis contributes to the formulation of policies by offering recommendations based on empirical evidence with regards to the attainment of energy security, curbing greenhouse gas emissions, and advancing the objectives of sustainable development (Xu et al., 2022).

Considering the first law of thermodynamics, the general energy balance equation is given as Eq. (2). Here, $\dot{Q}$ is the heat rate, $\dot{W}$ is the power, $\dot{m}$ is the mass flow rate, and h is the specific enthalpy.

$$\dot{Q} - \dot{W} = \sum \dot{m}_i h_i - \sum \dot{m}_o h_o \tag{2}$$

In addition, the energy balance equations are listed in Table 9 for all components used in the proposed process (Mofrad et al., 2023; Goswami, 2004).

The proposed process in this paper is a trigeneration structure, or, in other words, a CHP system which is also integrated using a seawater desalination cycle and fresh water production. Therefore, a very significant energy index for the proposed process is the energy utilization factor (EUF or f_{EU}), which is the sum of electrical efficiency (λ_{el}) and thermal efficiency (λ_{th}) and is defined based on Eq. (3) (Chicco and Mancarella, 2008a; Horlock, 1987).

$$f_{EU} = \lambda_{el} + \lambda_{th} \tag{3}$$

$$\lambda_{el} = \frac{\dot{W}_{net}^{Tri}}{\dot{Q}_{in}} \tag{4}$$

$$\lambda_{th} = \frac{\dot{Q}_{heat}}{\dot{Q}_{in}} \tag{5}$$

In Eqs. (4) and (5), $\dot{Q}_{in}$ represents the input energy to the structure, which is equal to the energy of the gas fuel flow (Eq. (7)) (Ji-chao and Sobhani, 2021). Furthermore, $\dot{W}_{net}^{Tri}$ is the net power generated (Eq. (6)) (Ji-chao and Sobhani, 2021), and $\dot{Q}_{heat}$ is the heat transfer rate of the heat exchangers (Eq. (8)) for hot water production, which is obtained through E-107, E-108, and E-104 heat exchangers. The heating value of the input fuel (LF biogas) is 8829 kJ/kg.

$$\dot{W}_{net}^{Tri} = \sum \dot{W}_T - \sum \dot{W}_C - \sum \dot{W}_p \tag{6}$$

$$\dot{Q}_{in} = \dot{m}_{fuel} \times LHV_{fuel} \tag{7}$$

$$\dot{Q}_{heat} = \dot{m}_{36} \times (h_{36} - h_{35}) + \dot{m}_{41} \times (h_{41} - h_{40}) + \dot{m}_{20} \times (h_{20} - h_{19}) \tag{8}$$

The second energy evaluation index for the proposed process being studied is primary energy savings (PES). This parameter demonstrates how much energy is saved by the proposed process compared to conditions where heat and power are produced separately, known as separation product (SP). PES is defined by Eq. (9). In Eq. (9), λ_{el}^{SP} and λ_{th}^{SP} are the electrical and thermal efficiency for the separation product, respectively, with values of 0.3 and 0.8, respectively (Chahartaghi and Sheykhi, 2018; Chicco and Mancarella, 2008a).

$$PES = 100 \times \left(1 - \frac{\dot{m}_{fuel} \times LHV_{fuel}}{\frac{\dot{W}_{net}}{\lambda_{el}^{SP}} + \frac{\dot{Q}_{heat}}{\lambda_{th}^{SP}}}\right) \tag{9}$$

In the following, according to the definition of efficiency of the first law of thermodynamics, equations related to the energy and electrical efficiency of subsystems are presented in Table 10.

4.2. Exergy analysis

Exergy analysis offers a comprehensive understanding of energy quality and potential utility within a given system, surpassing the conventional thermodynamic analysis that relies exclusively on energy balances (Chitgar et al., 2023). Considering this concept, it becomes feasible to uncover the ineffectiveness and wasted energy, thereby facilitating the suggestion of enhanced solutions across diverse sectors, including energy conversion, industrial operations, and environmental systems (Cao et al., 2020). In addition, exergy analysis optimizes the design of energy systems, facilitating the identification of promising

Table 2
Operational conditions of streams of the designed system.

Stream	T (°C)	P (kPa)	F (kmole/h)	Stream	T (°C)	P (kPa)	F (kmole/h)
1	25	1.01	5656	2	25	1.01	49,910
3	401.7	14.18	49,910	4	1124	14.18	49,910
5	517.3	1.01	49,910	6	451.8	1.01	55,570
7	1246	1.01	55,570	9	655.1	1.01	55,570
10	655.1	1.01	28,900	11	655.1	1.01	26,670
12	542	1.01	26,670	13	327.2	375	8180
14	549.9	375	81,800	15	362.8	75	8180
16	295.6	75	8180	17	203.3	75	8180
18	48.85	75	8180	19	25	1.01	31,050
20	55	1.01	31,050	21	200.8	375	8180
22	271.6	375	8180	23	327.2	375	8180
24	56.61	1.01	26,670	25	51.84	200	10,220
26	364.3	200	10,220	27	185.4	20	10,220
28	185.4	20	8648	29	185.4	20	1575
30	106.6	2.47	8648	31	47.29	20	1575
32	47.66	2.47	1575	33	105.7	2.47	10,220
34	26.99	2.47	10,220	35	25	1.01	132,800
36	54.95	1.01	132,800	37	29.82	200	10,220
38	51.84	200	10,220	39	39.54	1.01	26,670
40	25	1.01	5968	41	54.95	1.01	5968
52	90	1.01	28,900	43	85.9	20	4289
44	400	20	4289	45	332.3	0.2809	4289
45	332.3	0.2809	4289	46	84.96	0.2809	4289
47	85.9	20	4289	48	26.36	39	22,000
49	77.36	39	22,000	50	25.27	10.03	22,000
51	25.27	10.03	22,000	52	26.36	39	22,000
53	39.54	1.01	28,900	54	25	101.3	5000
55	27.25	0.2500	5000	56	65.39	0.2500	5000
57	65.39	0.2500	686.8	58	65.39	0.25	4313
59	54.43	0.15	4313	60	54.49	0.15	4313
61	55	0.25	686.8	62	54.49	0.15	780.9
63	54.49	0.15	3532	64	46.36	0.10	3532
65	46.46	0.10	3532	66	47	0.15	780.9
67	46.46	0.10	838.6	68	46.46	0.10	2694
69	46.01	0.10	2306	70	46.01	0.10	2306
71	44	1.01	28,900	72	35	0.10	2306
73	46	0.10	2306	74	44	1.01	26,670
75	44	1.01	55,570				

routes for advancement and searching for suitable energy conversion methods (Holagh et al., 2020). From the second law of thermodynamics, exergy is defined as the most useful work that can be obtained from a system in a particular state. Exergy is a property of the system, and it can also be described as the ability to do work.

The exergy of a stream includes both physical and chemical exergies (Azariyan et al., 2021).

$$e_i = e_i^{ph} + e_i^{ch} \tag{10}$$

The physical exergy of the stream of a substance can be defined as follows (Eq. (11)) (Mohammadi et al., 2018; Ghorbani et al., 2017):

$$e^{ph} = (h - h_0) - T_0(s - s_0) \tag{11}$$

where h_0 and s_0 are the enthalpy and entropy of the flow at ambient temperature and pressure. Chemical exergy for a substance stream is obtained from Eq. (12) (Ghorbani et al., 2020):

$$e^{ch} = \sum x_i e_i^0 + RT_0 \sum x_i \ln x_i \gamma_i \tag{12}$$

The parameter γ_i represents the activity factor for component i, which can be greater or less than 1. Chemical exergy can also be calculated through Gibbs free energy (Ghorbani et al., 2020; Azariyan et al., 2021). Furthermore, the exergy balance for equipment is calculated based on Eq. (13) in Table 11 (Fang et al., 2021). According to Eq. (13), exergy destruction equations are written for all equipment involved in the proposed process. Moreover, Eq. (14) (Nami et al., 2017) is used to determine the exergy efficiency of each component and the entire process's exergy efficiency. Similar to the first law of thermodynamics, using Eq. (14), the equations related to exergy efficiency for subsystems and the entire process are written (Table 12).

$$\dot{E}_F = \dot{E}_P + \dot{E}_D \tag{13}$$

$$\varphi_{ex} = \frac{\dot{E}_P}{\dot{E}_F} \tag{14}$$

4.3. Environmental analysis

CO_2 is a significant greenhouse gas predominant in global warming and the subsequent shifts in climatic conditions. Hence, comprehending and measuring CO_2 emissions is paramount in effectively monitoring energy systems' environmental ramifications (Liu et al., 2022a). Examining CO_2 emissions facilitates identifying and quantifying the distinct contributions made by various energy sources, fuels, and technologies to the overall level of emissions. Consequently, this analysis aids policymakers and researchers in placing greater importance on adopting low-carbon alternatives (Fang et al., 2023). Moreover, the analysis of CO_2 plays a crucial role in informing the progress and assessment of mitigation strategies specifically designed to decrease emissions of greenhouse gases (Cao et al., 2021a). The assessment of energy systems' efficiency and carbon intensity through CO_2 analysis serves to identify opportunities for improvement and optimize energy processes. Consequently, this aids in the transition towards energy systems that are more sustainable and environmentally friendly (Liu et al., 2022b).

Based on the proposed system, due to the presence of CO_2 in the input feed, it is necessary to determine the net total emission ($\beta_{net}^{CO_2}$) according to Eq. (15) for calculating the footprint parameter (Wei et al.,

Table 3
Characterization of the components used in the designed system.

Pumps					
Component	η_p (%)	$\dot{W}$ (kW)	P_{in} (kPa)	$\dot{m}_{in}$(kg /s)	P_{out} (kPa)
P-100	85	1627	247	50	20,000
P-101	85	551.7	28.09	136.1	2000
P-102	85	672.2	1003	104.1	3900
Heat Exchangers					
Component	LMTD (°C)	Heat duty (kW)	Min. approach (°C)	Hot Pinch Temp (°C)	Cold Pinch Temp (°C)
E-100	151.5	322,500	122.1	1246	1124.1
E-101	151.9	28,940	105.26	655.11	549.85
E-109	56.33	149,500	4.1	90	85.9
E-112	17.56	12,420	12.3	39.53	27.25
E-115	3.813	1092	2	46	44
E-117	3.81	1008	2	46	44
E-113	0.57	8283	3.52	55	54.4
E-114	2.94	9474	0.65	47	46.35
E-101	151.9	28,940	105.26	655.11	549.85
E-102	29.41	76,000	24	295.46	271.64
E-103	8.13	10,400	2.43	203.25	200.82
E-104	65.07	20,120	23.85	48.85	25
E-105	4.76	116,600	42.28	56.61	51.844
E-108	5.31	3861	1.66	56.61	54.95
E-106	56.77	4970	17.47	47.29	29.821
E-107	13.26	85,900	1.99	26.98	25
E-110	133.4	127,000	58.6	84.96	26.36
Turbine					
Component	η_T (%)	$\dot{W}$ (kW)	P_{in} (kPa)	$\dot{m}_{in}$(kg /s)	P_{out} (kPa)
T-100	85	281,700	1418	400	101
T-101	85	20,150	37,500	100	7500
T-102	85	18,290	20,000	50	2000
T-103	85	14,060	2000	42.16	247
T-105	85	15,740	3900	104.1	1003
Compressors					
Component	η_C (%)	$\dot{W}$ (kW)	P_{in} (kPa)	$\dot{m}_{in}$(kg /s)	P_{out} (kPa)
K-100	85	158,400	101	400	1418
K-101	85	11,330	37,500	100	7500
Interstage Coolers					
Component	T_{in} (°C)	T_{out} (°C)	ΔP (kPa)	$\dot{Q}$(kW)	$\dot{m}_{in}$(kg /s)
E-116	46	35	0.0	8729	11.54
E-111	25.27	25.27	0.0	111,900	104.1
Separators					
Component	T_{in}(°C)	T_{out} (°C)	ΔP (kPa)	$\dot{m}_l$(kg /s)	$\dot{m}_v$ (kg /s)
S-100	185.4	185.4	0.0	7.836	42.16
S-101	65.39	65.39	0.0	22.28	3.437
S-102	54.49	54.49	0.0	18.37	3.908
S-103	46.46	46.46	0.0	14.18	15.14

2023).

$$\beta_{net}^{CO_2}\left(\frac{kg_{CO_2}}{h}\right) = \xi_{CO_2} + \vartheta_{CO_2} - \Phi_{CO_2} \tag{15}$$

By determining the $\beta_{net}^{CO_2}$ parameter, the intensity of CO_2 emission (Ψ_{CO_2}) in the present process can be calculated using Eq. (16) (Ahmadi et al., 2013).

$$\Psi_{CO_2}\left(\frac{kg_{CO_2}}{kWh}\right) = \frac{\beta_{net}^{CO_2}}{\dot{W}_{net}^{Tri} + \dot{Q}_{heat} + \dot{E}_{heat}} \tag{16}$$

One of the crucial indices relevant to trigeneration structures is trigeneration CO_2 emission reduction (TCO_2ER), which indicates the percentage of CO_2 emission reduction in the proposed structure compared to a conventional SP process. It is defined by Eq. (17) (Chicco and

Table 5
Comparison of simulation results for the gas turbine and combustion chamber.

Parameters	Ji-chao and Sobhani (2021)	Current study	Relative error
Air inlet pressure (bar)	1.01	1.01	0.00
Air inlet temperature [K]	298.15	298.15	0.00
Chamber temperature [K]	1500	1519	1.25
Chamber pressure (bar)	1.01	1.01	0.00
Air preheat temperature [K]	1397.25	1397	0.02
Air temperature from compressor [K]	674.93	674.8	0.02
Gas temperature from preheater [K]	949.93	928.3	2.33
Turbine inlet temperature [K]	1397.25	1397	0.02
Turbine outlet temperature [K]	819.27	790.5	3.64

Table 6
Comparison of supercritical carbon dioxide cycle simulation results.

Parameters	Ji-chao and Sobhani (2021)	Current study	Relative error
Compressor outlet temperature [K]	442.96	474	6.55
Compressor outlet pressure [bar]	375	375	0.00
Turbine inlet pressure [bar]	375	375	0.00
Turbine inlet temperature [K]	823	823	0.00
Turbine outlet pressure [bar]	75	75	0.00
Turbine outlet temperature [K]	657.56	635.9	3.41
Evaporator inlet temperature [K]	627.5	600.3	4.53
Hot water temperature [K]	328.15	328.15	0.00
Compressor inlet temperature [K]	303.15	322	5.85

Table 4
Percentage composition of significant flows in the designed system.

Component	34	7	1	54	15	29	48
	Mole Fraction						
CO_2	0	0.0865	0.5000	0	1.0000	0	0
CH_4	0	0	0.3500	0	0	0	0
N_2	0	0.7249	0.1500	0	0	0	0
H2	0	0	0	0	0	0	0
O_2	0	0.1174	0	0	0	0	0
NH_3	0.4136	0	0	0	0	0.1040	1
H_2O	0.5864	0.0713	0	0.9876	0	0.8960	0
Octane	0	0	0	0	0	0	0
NaCl	0	0	0	0.0124	0	0	0

Table 7
Comparison of Kalina cycle simulation results.

Parameters	Ji-chao and Sobhani (2021)	Current study	Relative error
T-102 inlet pressure [bar]	200	200	0.00
T-102 outlet pressure [bar]	20	20	0.00
T-103 inlet pressure [bar]	20	20	0.00
T-103 outlet pressure [bar]	2.47	2.47	0.00
T-102 inlet temperature [K]	637.5	637.5	0.00
T-102 outlet temperature [K]	460.07	458.5	0.34
T-103 inlet temperature [K]	460.07	458.5	0.34
T-103 outlet temperature [K]	381.43	379.7	0.46
P-100 inlet pressure [bar]	2.47	2.47	0.00
P-100 outlet pressure [bar]	200	200	0.00
E-107 inlet temperature [K]	380.97	378.8	0.57
E-107 outlet temperature [K]	308.15	300.1	2.68
Expansion valve inlet pressure [bar]	20	20	0.00
Expansion valve outlet pressure [bar]	2.47	2.47	0.00

Table 8
Comparison of organic Rankine cycle using octane simulation results.

Parameters	Ahmadi et al. (2013)	This Study	Relative error
Turbine inlet/outlet temperature (°*C*)	400/335.7	400/329.1	0.00/2.01
Turbine inlet/outlet pressure (kPa)	2000/28.09	2000/28.09	0.00/0.00
pump inlet/outlet pressure (kPa)	28.09/2000	28.09/2000	0.00/0.00
pump inlet/outlet temperature (°*C*)	85/85	84.96/85.9	0.05/1.05
condenser inlet/outlet temperature (°*C*)	85/400	85.9/400	1.05/0.00

Mancarella, 2008a).

$$TCO2ER = 1 - \frac{\left(\mu^{F}_{CO2}\right)_{SP} \times \left(\dot{m}_{fuel} \times LHV_{fuel}\right)}{\left(\mu^{W}_{CO2}\right)_{SP} \times \dot{W}^{Tri}_{net} + \left(\mu^{Q}_{CO2}\right)_{SP} \times \dot{Q}} \tag{17}$$

$$\left(\mu^{Q}_{CO2}\right)_{SP} = \left(\mu^{F}_{CO2}\right)_{SP} \Big/ \lambda^{SP}_{th} \tag{18}$$

In Eq. (17), $(\mu^{F}_{CO2})_{SP}$ is the emission factor for fuel in the SP process, $(\mu^{W}_{CO2})_{SP}$ is the emission factor for power generation in the SP process, and $(\mu^{Q}_{CO2})_{SP}$ is the emission factor for heat production in the SP process. Eq. (18) defines the $(\mu^{Q}_{CO2})_{SP}$ parameter.

4.4. Economic analysis

Through assessing the costs and advantages associated with various energy sources and technologies, economic analysis facilitates the identification of economically feasible and environmentally sustainable solutions (Athari et al., 2022). This analysis facilitates the identification of market deficiencies and routes for enhancement within energy systems, thereby empowering policymakers to formulate efficient regulatory frameworks and incentive mechanisms. In general, economic analysis offers a quantitative and comprehensive comprehension of the complex interactions between energy systems and the economy, thus enabling the formulation of resilient energy policies and strategies (Jalili et al., 2022). In this study, an economic and thermo-economic analysis is performed on the proposed structure. Equations related to the basic economic and thermo-economic parameters are listed in Table 13. Additionally, economic assumptions are presented in Table 14. To calculate the FCI and TCI, Table 15 is used, which expresses costs as a function of the total equipment cost. The cost equations for heat exchangers, separators, the combustion chamber, turbines, compressors, and pumps are also listed in Table 16, where A is area (m^2), D is diameter, L is height, $\dot{m}$ is in kg/s, and temperature (T) is in Kelvin.

Table 9
Energy balance equations for equipment employed in the design system.

Components	Energy Equations
K-100	$\dot{m}_2h_2 + \dot{W} = \dot{m}_3h_3$
E-100	$\dot{m}_3h_3 + \dot{m}_7h_7 = \dot{m}_4h_4 + \dot{m}_9h_9$
T-100	$\dot{m}_4h_4 = \dot{W} + \dot{m}_5h_5$
CRV-100	$\dot{m}_6h_6 = \dot{m}_7h_7$
E-109	$\dot{m}_{10}h_{10} + \dot{m}_{43}h_{43} = \dot{m}_{42}h_{42} + \dot{m}_{44}h_{44}$
E-112	$\dot{m}_{42}h_{42} + \dot{m}_{55}h_{55} = \dot{m}_{53}h_{53} + \dot{m}_{56}h_{56}$
S-101	$\dot{m}_{56}h_{56} = \dot{m}_{57}h_{57} + \dot{m}_{58}h_{58}$
E-113	$\dot{m}_{59}h_{59} + \dot{m}_{57}h_{57} = \dot{m}_{60}h_{60} + \dot{m}_{61}h_{61}$
S-102	$\dot{m}_{60}h_{60} = \dot{m}_{62}h_{62} + \dot{m}_{63}h_{63}$
E-114	$\dot{m}_{62}h_{62} + \dot{m}_{64}h_{64} = \dot{m}_{66}h_{66} + \dot{m}_{65}h_{65}$
S-103	$\dot{m}_{65}h_{65} = \dot{m}_{67}h_{67} + \dot{m}_{68}h_{68}$
E-115	$\dot{m}_{53}h_{53} + \dot{m}_{69}h_{69} = \dot{m}_{70}h_{70} + \dot{m}_{71}h_{71}$
E-117	$\dot{m}_{70}h_{70} + \dot{m}_{39}h_{39} = \dot{m}_{73}h_{73} + \dot{m}_{74}h_{74}$
E-116	$\dot{m}_{73}h_{73} = \dot{Q} + \dot{m}_{72}h_{72}$
E-101	$\dot{m}_{11}h_{11} + \dot{m}_{13}h_{13} = \dot{m}_{12}h_{12} + \dot{m}_{14}h_{14}$
T-101	$\dot{m}_{14}h_{14} = \dot{W} + \dot{m}_{15}h_{15}$
E-102	$\dot{m}_{15}h_{15} + \dot{m}_{22}h_{22} = \dot{m}_{16}h_{16} + \dot{m}_{23}h_{23}$
E-103	$\dot{m}_{16}h_{16} + \dot{m}_{21}h_{21} = \dot{m}_{17}h_{17} + \dot{m}_{22}h_{22}$
E-104	$\dot{m}_{17}h_{17} + \dot{m}_{19}h_{19} = \dot{m}_{18}h_{18} + \dot{m}_{20}h_{20}$
K-101	$\dot{m}_{18}h_{18} = \dot{W} + \dot{m}_{21}h_{21}$
T-104	$\dot{m}_{44}h_{44} = \dot{W} + \dot{m}_{45}h_{45}$
E-110	$\dot{m}_{48}h_{48} + \dot{m}_{45}h_{45} = \dot{m}_{46}h_{46} + \dot{m}_{49}h_{49}$
T-105	$\dot{m}_{49}h_{49} = \dot{W} + \dot{m}_{50}h_{50}$
E-111	$\dot{m}_{50}h_{50} = \dot{Q} + \dot{m}_{51}h_{51}$
P-102	$\dot{m}_{51}h_{51} + \dot{W} = \dot{m}_{52}h_{52}$
P-101	$\dot{m}_{46}h_{46} + \dot{W} = \dot{m}_{47}h_{47}$
E-105	$\dot{m}_{12}h_{12} + \dot{m}_{25}h_{25} = \dot{m}_{26}h_{26} + \dot{m}_{24}h_{24}$
E-108	$\dot{m}_{40}h_{40} + \dot{m}_{24}h_{24} = \dot{m}_{39}h_{39} + \dot{m}_{41}h_{41}$
T-102	$\dot{m}_{26}h_{26} = \dot{W} + \dot{m}_{27}h_{27}$
S-100	$\dot{m}_{27}h_{27} = \dot{m}_{28}h_{28} + \dot{m}_{29}h_{29}$
T-103	$\dot{m}_{28}h_{28} = \dot{W} + \dot{m}_{30}h_{30}$
E-107	$\dot{m}_{33}h_{33} + \dot{m}_{35}h_{35} = \dot{m}_{36}h_{36} + \dot{m}_{34}h_{34}$
P-100	$\dot{m}_{34}h_{34} + \dot{W} = \dot{m}_{37}h_{37}$
VLV-100	$\dot{m}_{31}h_{31} = \dot{m}_{32}h_{32}$
E-106	$\dot{m}_{29}h_{29} + \dot{m}_{37}h_{37} = \dot{m}_{38}h_{38} + \dot{m}_{31}h_{31}$

Table 10
Equations related to the energy and electrical efficiency of the subsystems in the designed system.

Units	Equations
BPP	$\lambda_{el} = \lambda_{en} = \dfrac{\dot{W}_{net}}{\dot{m}_{fuel} \times LHV_{fuel}}$
SPU	$\lambda_{en} = \dfrac{\dot{W}_{net} + \dot{m}_{20} \times (h_{20} - h_{19})}{\dot{m}_{11} \times (h_{11} - h_{12})}$
SPU	$\lambda_{el} = \dfrac{\dot{W}_{net}}{\dot{m}_{11} \times (h_{11} - h_{12})}$
KC	$\lambda_{en} = \dfrac{\dot{W}_{net} + \dot{m}_{36} \times (h_{36} - h_{35})}{\dot{m}_{12} \times (h_{12} - h_{24})}$
KC	$\lambda_{el} = \dfrac{\dot{W}_{net}}{\dot{m}_{12} \times (h_{12} - h_{24})}$
OAPP	$\lambda_{el} = \dfrac{\dot{W}_{net}}{\dot{m}_{10} \times (h_{10} - h_{42})}$
Overall	$\lambda_{en} = \dfrac{\dot{m}_{20} \times (h_{20} - h_{19}) + \dot{m}_{36} \times (h_{36} - h_{35}) + \dot{m}_{41} \times (h_{41} - h_{40})}{\dot{m}_{fuel} \times LHV_{fuel}}$
Overall	$\lambda_{el} = \dfrac{\sum \dot{W}_T - \sum \dot{W}_C - \sum \dot{W}_P}{\dot{m}_{fuel} \times LHV_{fuel}}$

5. Results and discussion

In this section, first, the results obtained by the 4E analysis are provided, then the sensitivity study results are discussed.

Table 11
Equations of equipment exergy destruction.

Components	Exergy Equations
K-100	$\dot{E}_2 + \dot{W} - \dot{E}_3$
E-100	$\dot{E}_3 + \dot{E}_7 - \dot{E}_4 - \dot{E}_9$
T-100	$\dot{E}_4 - \dot{W} - \dot{E}_5$
CRV-100	$\dot{E}_6 - \dot{E}_7$
E-109	$\dot{E}_{10} + \dot{E}_{43} - \dot{E}_{42} - \dot{E}_{44}$
E-112	$\dot{E}_{42} + \dot{E}_{55} - \dot{E}_{53} - \dot{E}_{56}$
S-101	$\dot{E}_{56} - \dot{E}_{57} - \dot{E}_{58}$
E-113	$\dot{E}_{59} + \dot{E}_{57} - \dot{E}_{60} - \dot{E}_{61}$
S-102	$\dot{E}_{60} - \dot{E}_{62} - \dot{E}_{63}$
E-114	$\dot{E}_{62} + \dot{E}_{64} - \dot{E}_{66} - \dot{E}_{65}$
S-103	$\dot{E}_{65} - \dot{E}_{67} - \dot{E}_{68}$
E-115	$\dot{E}_{53} + \dot{E}_{69} - \dot{E}_{70} - \dot{E}_{71}$
E-117	$\dot{E}_{70} + \dot{E}_{39} - \dot{E}_{73} - \dot{E}_{74}$
E-116	$\dot{E}_{73} - \dot{E}_{72}$
E-101	$\dot{E}_{11} + \dot{E}_{13} - \dot{E}_{12} - \dot{E}_{14}$
T-101	$\dot{E}_{14} - \dot{W} - \dot{E}_{15}$
E-102	$\dot{E}_{15} + \dot{E}_{22} - \dot{E}_{16} - \dot{E}_{23}$
E-103	$\dot{E}_{16} + \dot{E}_{21} - \dot{E}_{17} - \dot{E}_{22}$
E-104	$\dot{E}_{17} + \dot{E}_{19} - \dot{E}_{18} - \dot{E}_{20}$
K-101	$\dot{E}_{18} + \dot{W} - \dot{E}_{21}$
T-104	$\dot{E}_{44} - \dot{W} - \dot{E}_{45}$
E-110	$\dot{E}_{48} + \dot{E}_{45} - \dot{E}_{49} - \dot{E}_{46}$
T-105	$\dot{E}_{49} - \dot{W} - \dot{E}_{50}$
E-111	$\dot{E}_{50} - \dot{E}_{51}$
P-102	$\dot{E}_{51} + \dot{W} - \dot{E}_{52}$
P-101	$\dot{E}_{46} + \dot{W} - \dot{E}_{47}$
E-105	$\dot{E}_{12} + \dot{E}_{25} - \dot{E}_{26} - \dot{E}_{24}$
E-108	$\dot{E}_{40} + \dot{E}_{24} - \dot{E}_{39} - \dot{E}_{41}$
T-102	$\dot{E}_{26} - \dot{W} - \dot{E}_{27}$
S-100	$\dot{E}_{27} - \dot{E}_{28} - \dot{E}_{29}$
T-103	$\dot{E}_{28} - \dot{W} - \dot{E}_{30}$
E-107	$\dot{E}_{33} + \dot{E}_{35} - \dot{E}_{36} - \dot{E}_{34}$
P-100	$\dot{E}_{34} + \dot{W} - \dot{E}_{37}$
VLV-100	$\dot{E}_{31} - \dot{E}_{32}$
E-106	$\dot{E}_{29} + \dot{E}_{37} - \dot{E}_{38} - \dot{E}_{31}$

Table 12
Equations related to the exergy efficiency of the subsystems and the exergy efficiency of the overall proposed process.

Units	Equations
BPP	$\varphi_{ex} = \frac{\dot{W}_{net}}{\dot{E}_{fuel}} = \frac{\dot{W}_{net}}{\dot{E}^{ph}_{fuel} + \dot{E}^{ch}_{fuel}}$
SPU	$\varphi_{ex} = \frac{\dot{W}_{net} + \dot{Q}_{E104} \times \left(1 - \frac{T_0}{T_H}\right)}{(\dot{E}_{11} - \dot{E}_{12})}$
KC	$\varphi_{ex} = \frac{\dot{W}_{net} + \dot{Q}_{E107} \times \left(1 - \frac{T_0}{T_H}\right)}{(\dot{E}_{12} - \dot{E}_{24})}$
OAPP	$\varphi_{ex} = \frac{\dot{W}_{net}}{(\dot{E}_{10} - \dot{E}_{42})}$
Overall	$\varphi_{ex} = \frac{\dot{Q}_{E107}\left(1 - \frac{T_0}{T_H}\right) + \dot{Q}_{E104}\left(1 - \frac{T_0}{T_H}\right) + \dot{W}_{net} + \dot{Q}_{E108}\left(1 - \frac{T_0}{T_H}\right)}{\dot{E}^{ph}_{fuel} + \dot{E}^{ch}_{fuel}}$
Overall	$\varphi^{th}_{ex} = \frac{\dot{Q}_{E107}\left(1 - \frac{T_0}{T_H}\right) + \dot{Q}_{E104}\left(1 - \frac{T_0}{T_H}\right) + \dot{Q}_{E108}\left(1 - \frac{T_0}{T_H}\right)}{\dot{E}^{ph}_{fuel} + \dot{E}^{ch}_{fuel}}$
Overall	$\varphi^{el}_{ex} = \frac{\sum \dot{W}_T - \sum \dot{W}_C - \sum \dot{W}_P}{\dot{E}^{ph}_{fuel} + \dot{E}^{ch}_{fuel}}$

5.1. Energy analysis results

The overall energy efficiency of the new process is represented by the parameter EUF. In addition, Fig. 4 illustrates the energy flow diagram, and in Fig. 5, the energy (λ_{en}) and electrical efficiency for subsystems are compared. According to Fig. 4, the total input energy into the new

Table 13
Equations related to basic economic and thermo-economic parameters.

Parameters	Equation
Fixed capital investment ($) (Liu et al., 2023)	Direct cost + indirect cost
Total capital investment ($) (Liu et al., 2023; Sarcheshmehpoor, 2019)	Other Outlays + Fixed capital investment
Total annual cost ($/year) (Gu et al., 2023)	(Direct cost + indirect cost) × CRF + Energy Cost
capital recovery factor (Mohammadi et al., 2023)	$\frac{i \times [i+1]^n}{[1+i]^n - 1}$
Net present value ($) (Ahmadi et al., 2020; Tzivanidis et al., 2016)	$-\text{TCI} + \left[\text{cash flow} \times \frac{(1+i)^n - 1}{i \times (i+1)^n}\right]$
total product cost ($/GJ) (Gu et al., 2023; Cao et al., 2021b)	$\text{CRF} \times \text{TCI} \times \alpha \times \frac{1}{t_y \times \text{exergy product}}$
Cost of Energy ($/kWh) (Mores et al., 2014)	$\frac{\text{TAC}}{t_y \times \text{energy product}}$

Table 14
Assumptions considered in economic estimates.

Parameters	Value
the interest rate (i) (Ji-chao and Sobhani, 2021; Mohammadi et al., 2023)	0.12
total operating time (t_y) (Mohammadi et al., 2023)	8000
Maintenance factor (α) (Ji-chao and Sobhani, 2021)	1.06
Plant expected life (n) (Ji-chao and Sobhani, 2021)	20 years
Cooling water cost (Wei et al., 2023)	0.354 $/GJ

Table 15
Coefficients related to direct and indirect cost estimates (Ahmadi et al., 2013; Sarcheshmehpoor, 2019).

I. Fixed-Capital Investment (FCI)	
A. Direct Costs (DC)	
A.1. Onsite Costs (ONSC)	
Purchased-Equipment installation	90% PEC
Purchased-Equipment Cost (PEC)	PEC
Instrumentation and Controls	40% PEC
Piping	70% PEC
Electrical Equipment and materials	15% PEC
A.2. Offsite Costs (OFSC)	
Land	10% PEC
Service facilities	100% PEC
Civil, structural and architectural work	90% PEC
Total direct costs (DC) = (ONSC) + (OFSC)	
B. Indirect Costs (IC)	
B.1. Contingencies	25% sum of above
B.2. Construction costs	15% DC
B.3. Engineering and supervision	75% PEC
Total indirect costs (IC)	
II. Other Outlays	
Allowance for funds used during construction	15% FCI
Working capital	20% TCI
Startup costs	12% FCI

Table 16
Equations for estimating the cost of employed equipment.

Components	Equations
turbine (Cavalcanti, 2017)	$2210 \times \dot{W}^{0.7}$
Compressor (Liu et al., 2023)	$91562 \times \left[\frac{\dot{W}}{445}\right]^{0.67}$
Exchangers (Dincer et al., 2017)	$10^3 \times A^{0.65}$
Pump (Mahmoudan et al., 2022)	$3540 \times \dot{W}^{0.71}$
Chamber (Sadat et al., 2020)	$\frac{[1 + e^{(0.018T_{72} - 26.4)}]46.08 \times \dot{m}_{in}}{0.995 - \frac{P_i}{P_o}}$
Separator (Hai et al., 2023)	$17640 \times D^{1.06}(m) \times L^{0.802}(m)$

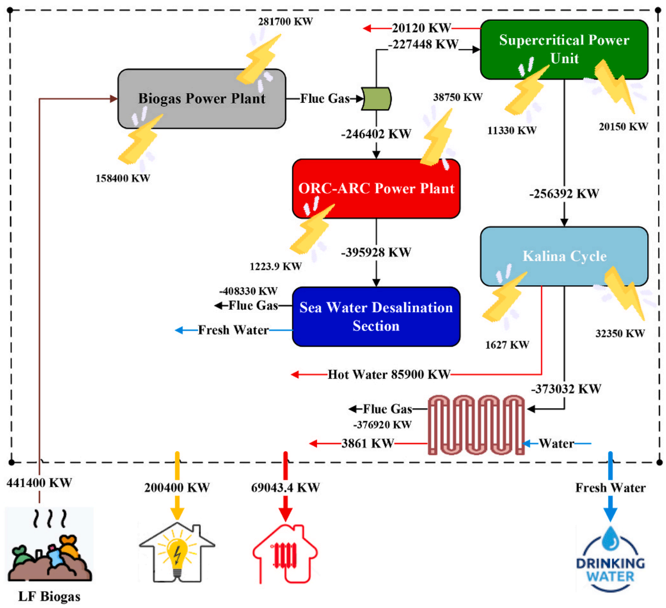

Fig. 4. Energy flow diagram for the designed system.

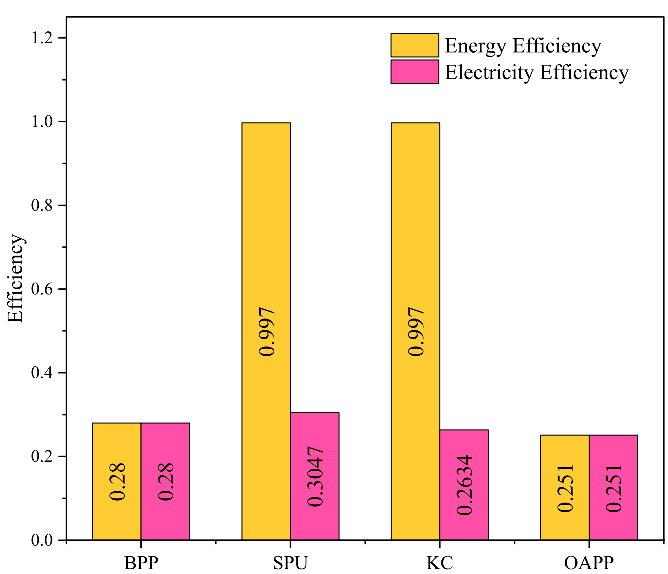

Fig. 5. Comparison of electrical efficiency and energy efficiency of subsystems.

structure is equal to 441,400 kW, and the proposed structure, based on the predicted configuration, can produce its own products, which are fresh water, electricity, and heat, at rates of 11.54 kg/ s, 200,400 kW, and 69,043.4 kW (55 °C hot water), respectively. Based on Fig. 4, the overall results for evaluating the first law of thermodynamics are listed in Table 17.

According to Fig. 5, it can be concluded that:

- Among the subsystems, the SPU subsystem has the highest electrical efficiency (30.47%) and the OAPP section has the lowest electrical efficiency (25.1%).
- The comparison of the results indicates that the Kalina cycle is more efficient than the combination of the ORC and the ARC.
- Based on the energy efficiency values for the SPU and KC sections, it is clear that heat recovery and heating production bring the efficiency close to 100%, indicating the importance of heat recovery.
- Based on the analysis, the OAPP section is the least efficient cycle in the proposed process.

Table 17
The overall results of the evaluation of the first law of thermodynamics for the designed system.

Biogas Power Plant	
Gross electricity produced (kW)	281,700
Net electricity produced (kW)	123,300
Energy inlet (kW)	441,400
Supercritical Power Unit	
Gross electricity produced (kW)	20,150
Net electricity produced (kW)	8820
Energy inlet (kW)	28,944
Heating product (kW)	20,120
ORC-ARC Power Plant	
Gross electricity produced (kW)	38,750
Net electricity produced (kW)	37,526.1
Energy inlet (kW)	149,526
Kalina Cycle	
Gross electricity produced (kW)	32,350
Net electricity produced (kW)	30,723
Energy inlet (kW)	116,640
Heating product (kW)	85,900
Overall Process	
Electric efficiency [%]	45.39
Thermal efficiency [%]	24.89
Energy utilization factor [%]	70.28
Primary energy saving [%]	45.18

Tables 18–20 compare important indicators for evaluating the first law of thermodynamics with other studies. Regarding electrical efficiency, Table 12 shows that the proposed structure has superiority over other studies and methods. Also, the comparison of EUF indicates that the proposed structure is much better in terms of energy efficiency than other methods. This superiority is very significant compared to CHP systems based on biomass and renewable energy sources (Table 13). Furthermore, as shown in Table 14, the present process achieves substantial fuel savings (PES index) compared to similar multi-generation systems (Mohammadi et al., 2018; Haghghi et al., 2023), and this increase is noteworthy.

5.2. Exergy analysis results

Fig. 6 shows the exergy flow diagram for the proposed process. According to this figure, the total input exergy (LF biogas fuel exergy) is equal to 475,850.44 kW, out of which kW 200,400 power, kW 8504.73 heat, and 11.54 kg/s of fresh water are produced. Based on Fig. 6, the overall results related to the exergy evaluation are reported in Table 21.

According to exergy analysis, it is found that the proposed scheme has an overall exergy efficiency of 57.51%, an electrical exergy efficiency of 54.77%, and a thermal exergy efficiency of 2.74%. Furthermore, the exergy efficiencies of subsystems are compared in Fig. 7. This figure shows that KC and BPP subsystems have the highest and lowest efficiencies with values of 0.7142 and 0.259, respectively. Based on Fig. 7, among the two systems SPU and KC, KC has a higher exergy efficiency and better thermodynamic performance for power generation through waste heat recovery. In Table 22, the exergy efficiency of various multi-generation systems that utilize different energy sources is compared. The results indicate that using the biogas combustion method

Table 18
Comparison of electrical efficiency with other studies.

Other studies	Process	λ_{el} [%]
Mehrpooya et al. (2017)	CCHP with Stirling engine and molten carbonate fuel cell	42.28
Chahartaghi and Sheykhi (2018)	Trigeneration scheme relying on beta-type Stirling engine	27.31
Bamisile et al. (2019)	Renewable energy-based trigeneration arrangement	43.96
This study	Integrated trigeneration system based on landfill biogas	45.39

Table 19
Comparison of energy efficiency (EUF index) with other studies.

Other studies	Process	f_{EU} [%]
Safari and Dincer (2019)	Biomass-based multigeneration arrangement	63.6
Siddiqui and Dincer (2021)	Bio-waste-based multigeneration arrangement	66.4
Gu et al. (2023)	Power and methanol cogeneration arrangement using CO_2 capture and heat recovery	64.13
Liu et al. (2023)	Multigeneration system using oxyfuel combustion and geothermal energy	47.2
Ogorure et al. (2018)	Integrated multigeneration thermal power plant	63.62
Bellos and Tzivanidis (2021)	Solar-driven trigeneration system	37.34
This study	Integrated trigeneration system based on landfill biogas	70.28

Table 20
Comparison of the PES index with other studies.

Other studies	Process	PES[%]
Cao et al. (2022)	Trigeneration scheme relying on beta-type Stirling engine	31.83
Chahartaghi and Sheykhi (2018)	Multigeneration arrangement	18
This study	Integrated trigeneration system based on landfill biogas	45.18

and harnessing the energy of combustion gases leads to an increase in the system's thermodynamic efficiency compared to when the gasification method (He et al., 2023; Ji-chao and Sobhani, 2021; Ahmadi et al., 2013) or solar/hybrid sources (Hashemian and Noorpoor, 2019; Sezer and Koç, 2019) are used.

Table 23 presents the results of exergy destruction estimation and exergy efficiency of equipment. According to this table, the total exergy destruction in the proposed system is 339,006 kW, and among the subsystems, the biogas combustion and power generation BPP unit has the most irreversibility with an exergy destruction of 183,501 kW (61% as shown in Fig. 8). Fig. 8 shows that the fresh water production subsystem has the lowest irreversibility with a 1% share. Also, based on the results of Table 23, among the heat exchangers used for heat recovery, the E-103 heat exchanger in the supercritical CO_2 cycle has the highest efficiency. Furthermore, in the overall proposed process, the CRV-100

Table 21
The overall results of the evaluation of the second law of thermodynamics for the proposed process.

Biogas Power Plant	
Gross electricity produced (kW)	281,700
Net electricity produced (kW)	123,300
Exergy inlet (kW)	475,850.44
Supercritical Power Unit	
Gross electricity produced (kW)	20,150
Net electricity produced (kW)	8820
Exergy inlet (kW)	19,029.6
Heating Exergy product (kW)	1557.28
ORC-ARC Power Plant	
Gross electricity produced (kW)	38,750
Net electricity produced (kW)	37,526.1
Exergy inlet (kW)	76,157.64
Kalina Cycle	
Gross electricity produced (kW)	32,350
Net electricity produced (kW)	30,723
Exergy inlet (kW)	52,326.22
Heating Exergy product (kW)	6648.61
Overall Process	
Electric Exergy efficiency [%]	54.77
Thermal Exergy efficiency [%]	2.74
Total Exergy Efficiency [%]	57.51

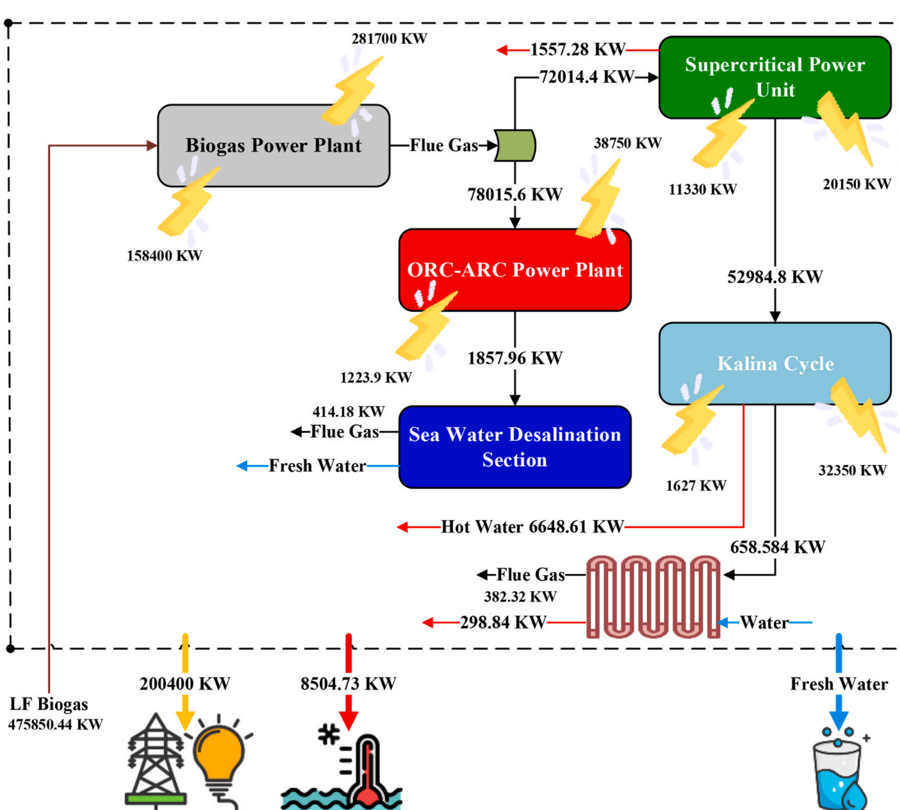

Fig. 6. Exergy flow diagram for the trigeneration process.

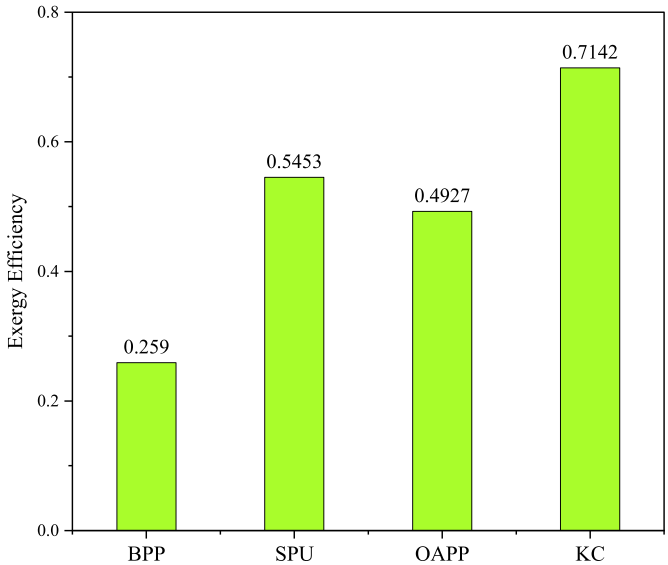

Fig. 7. Comparison of subsystems exergy efficiency.

Table 22
Comparison of overall exergy efficiency with other studies.

Other studies	Process	φ_{ex}[%]
He et al. (2023)	Multigeneration arrangement relying on biogas-steam reforming	31.14
Hashemian and Noorpoor (2019)	Solar and biomass-based multigeneration arrangement	14
Ji-chao and Sobhani (2021)	Biomass-based multigeneration arrangement	40.97
Ahmadi et al. (2013)	Biomass-based multigeneration arrangement	22.2
Mohammadi et al. (2023)	Multigeneration arrangement based on solar and geothermal energies	25.4
Xue et al. (2022)	Biomass-based multigeneration arrangement	16.72
Sezer and Koç (2019)	Multigeneration arrangement based on wind and solar energies	30.6
This study	Integrated trigeneration system based on landfill biogas	57.51

combustion chamber in the biogas combustion gas turbine cycle has the highest exergy destruction (42.22%).

5.3. Environmental analysis results

In Fig. 9, the CO_2 emission flow diagram of the trigeneration process is presented. According to this plot, LF biogas fuel, which contains 124,470.37 kg/h of CO_2 (Φ_{CO_2}) before combustion in the combustor, reaches 211,599.62 kg/h of CO_2 after combustion. Of this amount of CO_2 present in the exhaust gas, 110,031.8 kg/h is sent to the OAPP subsystem.

The remaining flue gas, with a CO_2 content of 101,567.82 kg/ h, is directed to the SPU subsystem. Except in the BPP section, the CO_2 content in other subsystems remains unchanged, and due to heat integration, the total indirect emissions (ξ_{CO_2}) from this system are zero. Since the ξ_{CO_2} parameter is zero, therefore, the value of $\beta_{net}^{CO_2}$ is equal to the direct emissions (ϑ_{CO_2}), which according to Fig. 9, is equal to 87,129.25 kg/h.

According to Eq. (16), the Ψ_{CO_2} parameter for the proposed process is equivalent to 0.272 kg_{CO_2}/kWh, and this value is compared with other studies in Table 24. Table 24 shows the proposed structure has a lower diffusion intensity than multi-generational methods that use biomass or biogas energy sources.

Additionally, the $(\mu_{CO2}^{W})_{SP}$ and $(\mu_{CO2}^{F})_{SP}$ parameters are 0.836 kg_{CO_2}/ kWh and 0.22 kg_{CO_2}/kWh, respectively (Chahartaghi and Sheykhi,

Table 23
Results of exergy destruction rate (kW) calculation for the proposed process.

Components	$\dot{E}_F$	$\dot{E}_P$	$\dot{E}_D$	φ_{ex}^{i}
Biogas Power Plant (BPP)				
K-100	158,400	147,320	11,080	0.93
E-100	250,200	233,200	17,000	0.932
T-100	294,000	281,700	12,300	0.958
CRV-100	590,322	447,201	143,121	0.76
ORC/ARC Power Plant (OAPP)				
E-109	76,159	62,444	13,715	0.82
T-104	24,280	23,010	1270	0.947
E-110	38,607	17,041	21,566	0.44
T-105	17,499	15,740	1759	0.899
E-111	33,624	33,447	177	0.99
P-102	672	625	52	0.93
P-101	552	544	8	0.985
Supercritical Power Unit (SPU)				
E-101	80,797	16,700	64,097	0.21
T-101	21,220	20,150	1070	0.949
E-102	3900	3640	260	0.933
E-103	4540	4290	250	0.945
E-104	4650	950	3700	0.204
K-101	11,330	9520	1810	0.84
Kalina Cycle (KC)				
E-105	52,326	19,635	32,691	0.375
T-102	19,615	18,290	1325	0.932
S-100	29,200	29,120	80	0.997
T-103	15,346	14,060	1286	0.916
E-107	11,923	4046	7877	0.339
P-100	1627	1347	280	0.827
E-106	1139	249	890	0.22
VLV-100	45	29	16	0.644
Sea Water Desalination Section (SWDS)				
E-112	1444	1260	184	0.873
S-101	1260	1200	60	0.952
E-115	77	54	23	0.701
E-113	980	745	235	0.76
S-102	970	954	16	0.984
E-114	842	634	208	0.753
E-117	646	53	593	0.082
E-116	2006	1999	7	0.997

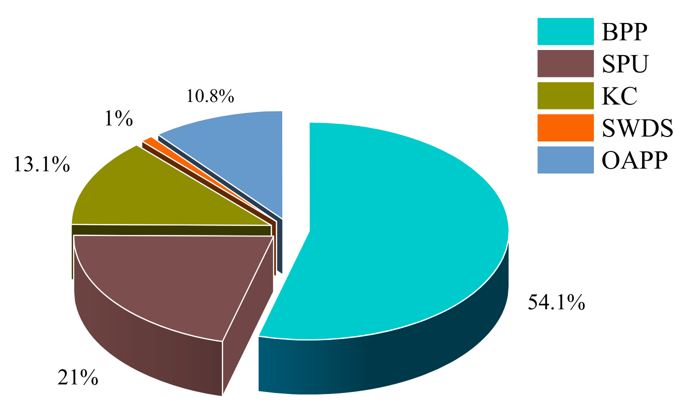

Fig. 8. Comparison of subsystems exergy destruction.

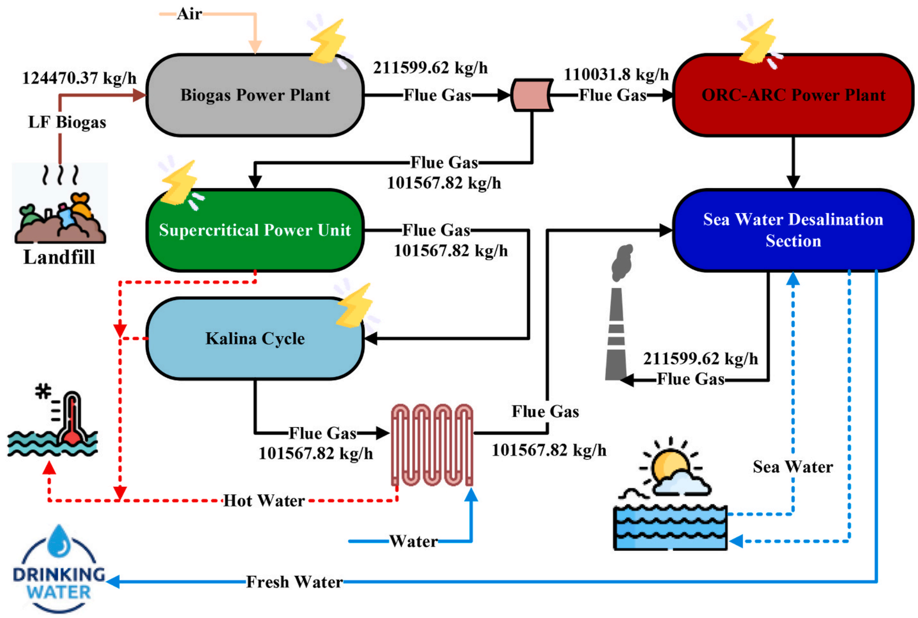

Fig. 9. Carbon dioxide flow diagram for the proposed process.

Table 24
Comparison of the Ψ_{CO_2} environmental index with other studies.

Studies	Process	Ψ_{CO_2} [kg_{CO_2} /kWh]	Reduction [%]
Ahmadi et al. (2013)	Biomass-driven multigeneration arrangement	0.519	47.59
Baghernejad et al. (2016)	SOFC-based multigeneration arrangement	0.363	25.06
Baghernejad et al. (2016)	Biomass-driven trigeneration arrangement	0.639	57.43
This study	Integrated trigeneration system based on landfill biogas	**0.272**	–

Table 25
Overall results of the environmental assessment for the proposed structure.

Parameter	Value
Direct emission	211,599.62
Indirect emission	0.0
Total CO_2 emission	211,599.62
Total Net CO_2 emission	87,129.25
Specific CO_2 emission (kg_{CO_2} / kWh)	0.272
TCO_2ER (%)	51.02

2018). Table 25 presents the overall results of the environmental assessment for the proposed structure.

5.4. Economic analysis results

Table 26 presents the results of calculating the total cost for all equipment, which amounts to $55,781,510. Also, results of estimating direct and indirect costs are given in Table 27. Additionally, the total investment cost of the project is equivalent to $523,267,174 (overall results are shown in Table 28). The values of total produced energy, exergy, and power from the proposed structure were obtained in the thermodynamic evaluation section. Based on these values, three parameters, "cost of energy," "cost of electricity," and "TUCP," are calculated as 0.022 $/kWh, 0.034 $/kWh, and 12.25 $/GJ, respectively. The NPV value shows that this structure has economic growth potential, and its profitability is $779,571,045. Table 29 compares the TUCP competitive index with other studies. According to Table 29, the proposed structure has lower exergy production costs compared to methods based on biomass, gasification, and produced gas combustion (Behzadi et al., 2020; Sadeghi et al., 2018), as well as renewable energies (Mahmoudan

Table 26
Results of estimating the cost of used equipment.

Components	Value ($)
E-116	360,500
E-104	515,600
T-103	1,770,036
E-108	1,620,300
S-100	164,400
E-112	1,681,900
T-105	1,915,559
E-102	172,949
E-105	752,125
E-111	903,900
E-106	240,800
P-100	1,310,800
E-113	529,200
S-103	173,900
T-100	11,420,227
K-101	801,029
T-101	2,170,114
E-109	13,088,500
K-100	4,689,754
S-102	171,000
E-103	370,887
E-114	958,900
E-100	965,804
E-115	654,100
E-117	479,400
P-102	381,900
T-104	2,498,814
P-101	407,300
E-107	1,214,800
E-101	194,356
T-102	2,127,854
E-110	552,400
S-101	177,300
CRV-100	345,102
Total equipment cost	**55,781,510**

Table 27
Results of estimating direct and indirect costs.

A. Direct Costs (DC)	
A.1. Onsite Costs (ONSC)	
Purchased-Equipment installation	50203359
Purchased-Equipment Cost (PEC)	55781510
Instrumentation and Controls	22312604
Piping	39047057
Electrical Equipment and materials	8367227
A.2. Offsite Costs (OFSC)	
Land	5578151
Service facilities	55781510
Civil, structural and architectural work	50203359
Total direct costs (DC) = (ONSC) + (OFSC)	287274777
B. Indirect Costs (IC)	
B.1. Contingencies	21231838
B.2. Construction costs	43091217
B.3. Engineering and supervision	41836133
Total indirect costs (IC)	106159188
II. Other Outlays	
Allowance for funds used during construction	59015095
Working capital	104653435
Startup costs	47212076

Table 28
Overall results of the economic evaluation of the proposed process.

Parameters	Value
Fixed capital investment ($)	393,433,965
Total capital investment ($)	523,267,174
Total annual cost ($/ year)	53,902,736
total product cost ($/ GJ)	12.25
Cost of Energy ($/ kWh)	0.022
Cost of Electricity ($/ kWh)	0.034
Net present value ($)	779,571,045

Table 29
Comparison of the TUCP index with other studies.

Other studies	Process	TUCP [$ /GJ]
Behzadi et al. (2020)	Biomass-driven fuel cell-based multigeneration arrangement	69.47
Mohammadi et al. (2023)	Solar and geothermal-based multigeneration arrangement	37.8
Mohammadi et al. (2023)	Multigeneration arrangement based on solar and geothermal energies	34.1
Sadeghi et al. (2018)	Biomass-driven fuel cell-based multigeneration arrangement	33.99
This study	Integrated trigeneration system based on landfill biogas	12.25

et al., 2022).

5.5. Sensitivity analysis results

Fig. 10 illustrates the variations in thermodynamic efficiencies and the primary energy storage (PES) index in terms of the changes in the outlet pressure of the T-100 turbine. Based on the analysis conducted, increasing the outlet pressure of the gas turbine leads to a decrease in the overall thermodynamic performance of the system and a reduction in the PES index. The main reason for this is the decrease in overall net power generation ($\dot{W}_{net}^{Tri}$), which results in a decreased suitable utilization of input energy.

In addition, according to Fig. 11, as the outlet pressure of the gas turbine increases, the SCE environmental index also increases, and the amount of CO_2 emissions reduction compared to the SP process (TCO_2ER) decreases, both indicating an increase in system pollution. The SCE index has an inverse relationship with the amount of energy and exergy produced, and as mentioned, with an increase in turbine outlet pressure, the parameter $\dot{W}_{net}^{Tri}$ decreases. Therefore, under conditions where direct CO_2 emissions are constant, the intensity of pollution

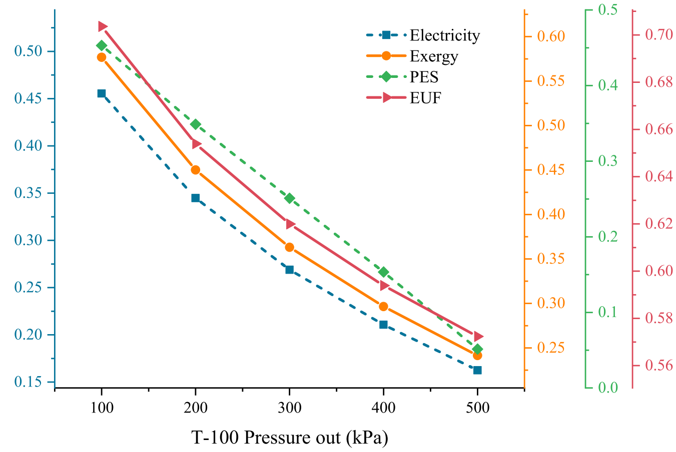

Fig. 10. The effect of gas turbine outlet pressure on the overall thermodynamic efficiencies of the system.

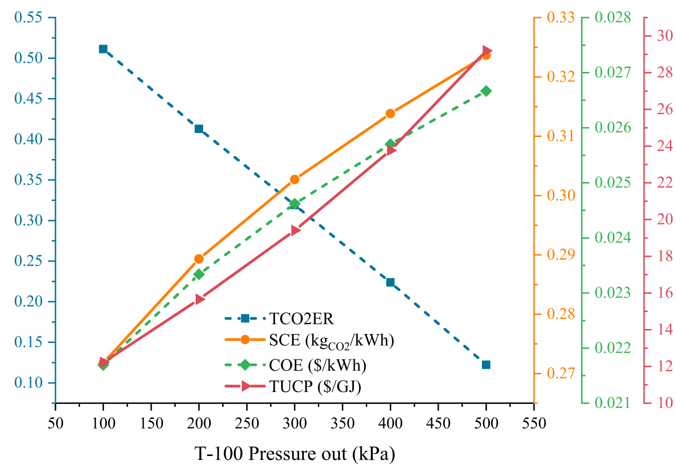

Fig. 11. The effect of gas turbine outlet pressure on CO_2 footprint and the TCO_2ER thermo-environmental index and thermo-economic indices of the proposed process.

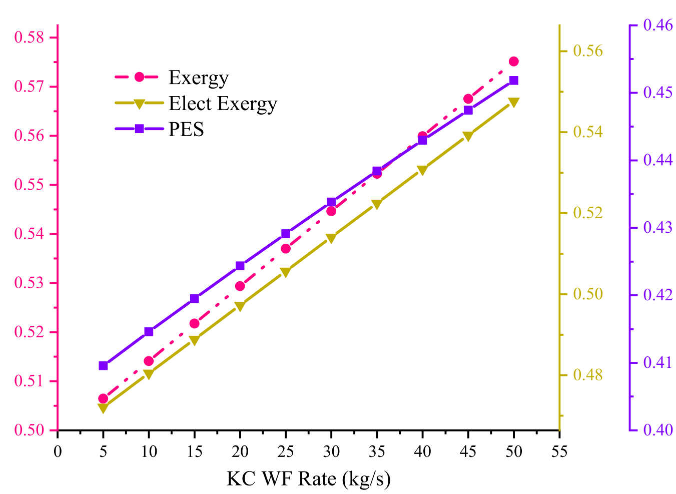

Fig. 12. The effect of the flow rate of Kalina cycle working fluid on the PES index and thermodynamic efficiencies.

increases, and due to this decrease in energy production, the TCO_2ER parameter declines. Fig. 11 also shows that both TUCP and COE indices increase with an increase in turbine outlet pressure, which is undesirable because products are produced at a higher cost. Both COE and TUCP indices have an inverse relationship with the $\dot{W}_{net}^{Tri}$ parameter (according to Table 22 equations). Therefore, as power production decreases, their trend increases. Accordingly, based on the results of the analysis, it is preferable that the gas turbine outlet pressure does not increase (see Fig. 12).

The second key parameter under investigation is the working fluid flow rate in the Kalina cycle. Fig. 13 indicates that increasing the fluid flow rate improves thermodynamic performance and the PES index. The reason for this is an increase in power production and cooling, which leads to an increase in overall exergy efficiency and electrical exergy efficiency. In addition, increasing the working fluid flow rate in the KC subsystem enhances the TCO_2ER index (Fig. 13), which is due to an improvement in the overall thermodynamic efficiency of the proposed process since TCO_2ER depends on the energy produced, according to Eq. (17).

As mentioned earlier, increasing the flow rate of the working fluid in the KC subsystem leads to an increase in total net power generation and exergy efficiency. Increasing exergy efficiency while exergy availability remains constant means an increase in exergy production. As a result, these changes ultimately lead to a decrease in the TUCP competitive index (Fig. 13). In Figs. 14 and 15, the variations of thermodynamic efficiency and thermo-economic indices are investigated as functions of inlet flue gas temperature in the SWDS section. According to Fig. 14, increasing the flue gas temperature as the driving force of the SWDS subsystem decreases the overall thermodynamic efficiency of the process and reduces energy storage compared to the SP process. The main reason for this issue is the reduction in power generation in the proposed process turbines since less flue gas energy is directed towards the SPU and OAPP subsystems. Moreover, the decrease in thermodynamic efficiency is inversely related to measures such as TUCP and COE due to the reduction in product production. Therefore, despite an increase in fresh water production, raising the temperature of the input flue gas to the SWDS will result in lower thermodynamic efficiency, reduced energy storage, and increased production costs.

6. Conclusion

This study proposes an innovative structure that utilizes landfill biogas fuel. The proposed structure is modeled using Aspen HYSYS software, and various analyses such as energy, exergy, economic, and environmental are conducted. Parametric studies and comparison of results with other research papers are also performed to explain the superiority of this novel process. The process structure is completely new, and the system undergoes thermal integration through the supercritical CO_2 cycle, ORC, ARC, sea water desalination unit, and Kalina cycle. Additionally, to improve heat recovery performance, the energy available in the process is used to produce hot water via several heat exchangers. The following is a summary of the results of this study:

- The thermodynamic evaluations indicate that the energy utilization factor (EUF), exergy efficiency, and thermal efficiency are 70.28%, 57.51%, and 24.89%, respectively.
- Evaluations show that the TCO_2ER index for the proposed process is 51.02%. The parametric study demonstrates that the increase in gas turbine outlet pressure and the increase in the temperature of the input heat source to the seawater desalination subsystem are two factors that reduce this competitive index.
- Environmental assessment shows that there is no indirect emission for the proposed structure (due to the heat integration network) and the parameter $\beta_{net}^{CO_2}$ is equal to 87,129.25 kg/h. Comparison of CO_2 emission intensity (0.272 kg_{CO_2}/kWh) with other studies indicates the superiority of the environmental performance of the proposed structure.

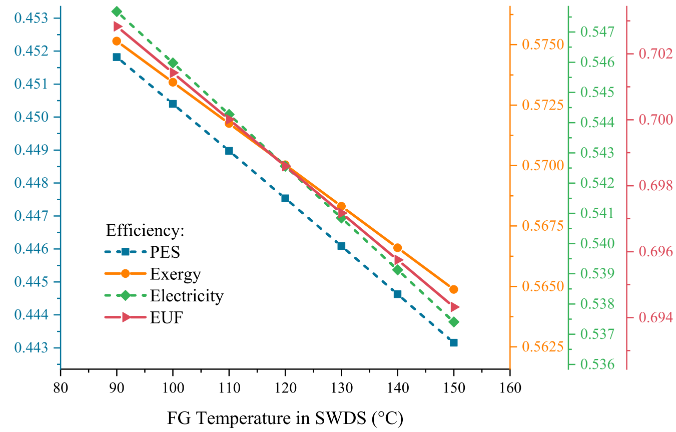

Fig. 14. The effect of flue gas temperature in the desalination section on thermodynamic parameters.

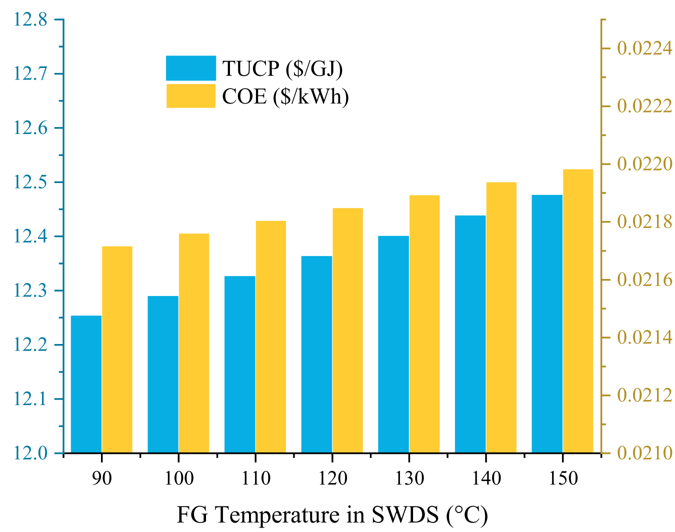

Fig. 15. The effect of flue gas temperature in the desalination section on thermo-economic indices of the process.

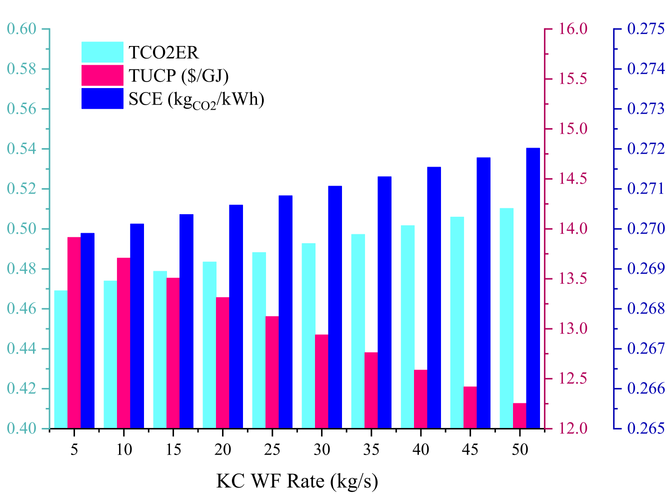

Fig. 13. The effect of the flow rate of Kalina cycle working fluid on the TCO_2ER thermo-environmental and the TUCP thermo-economic index.

- The economic analyses indicate that the total unit cost of products and the cost of energy for the proposed structure are 12.25 $/ GJ and 0.022 $/kWh, respectively. The parametric evaluation explains that increasing the flue gas temperature entering the SWDS and the gas turbine's output pressure are factors that challenge the mentioned indices. However, increasing the working fluid flow rate in the Kalina cycle reduces both parameters.
- Parametric studies describe that by increasing the outlet pressure of the gas turbine and increasing the heat source temperature in the desalination unit, the thermodynamic and thermo-economic performance of the proposed structure decreases, mainly due to the reduction in net power generation.

The present study encompasses certain limitations and practical constraints, which are outlined hereafter:

- The existing system necessitates the availability and ease of access to landfill gas resources to operate effectively. Hence, the efficient collection and segregation of municipal waste is crucial in ensuring a consistent and dependable supply of input fuel to the proposed system.
- The proposed system demonstrates elevated initial expenses related to installation and configuration. Despite the favorable economic outcomes observed during the implementation of the system, the project may face potential restrictions due to the significant upfront expenses.
- The geographical scope of system deployment is restricted primarily to coastal regions and areas with access to seawater sources due to the utilization of the desalination cycle and the subsequent production of fresh water.
- According to the combined framework of the proposed system, more attention to heat recovery components is needed to ensure the sustainability and productivity of the system. Therefore, it is imperative that the skilled workforce consistently evaluates the operational variables in tandem with advanced machinery.

In addition, it is recommended that future studies investigate the subsequent subjects:

- It is recommended to utilize fossil/hydrocarbon fuels rather than biogas fuel for the purpose of conducting a comparative analysis of the attained outcomes.
- It is advisable to apply the life cycle assessment (LCA) to comprehensively evaluate the proposed model from an environmental viewpoint.
- It is advisable to perform a range of optimization scenarios, employing thermodynamic, cost, and environmental criteria, to achieve the system's most efficient performance.

CRediT authorship contribution statement

Wu Shao: Resources, Formal analysis, Investigation, Writing and editing-revised draft, Supervision, Methodology. **Ayman A. Ghfar:** Methodology, Writing – original draft, Project management, Investigation, Resources. **Aliashim Albani:** Writing – review & editing, Methodology, Formal analysis, Data curation. **Manoj Kumar Agrawal:** Methodology, Writing – original draft, Data curation, Resources. **Fahid Riaz:** Writing and editing-revised draft, Supervision, Resources. **Kwanho Shi:** Writing and editing-revised draft, Supervision.

Declaration of competing interest

The authors declare that they have no known competing financial interests or personal relationships that could have appeared to influence the work reported in this paper

Data availability

Data will be made available on request.

Acknowledgments

The Natural Science Foundation of Hunan Province: Research on Key control technology of quasi-Z-source cascade photovoltaic system (2023JJ50263).

The authors are grateful to the Researchers Supporting Project number (RSP2023R407), King Saud University, Riyadh, Saudi Arabia, for the financial support.

Authors acknowledge financial support from Abu Dhabi University's Office of Research and Sponsored Programs.

References

Ahmadi, P., Dincer, I., Rosen, M.A., 2013. Development and assessment of an integrated biomass-based multi-generation energy system. Energy 56, 155–166.
Ahmadi, A., Assad, M.E.H., Jamali, D.H., Kumar, R., Li, Z.X., Salameh, T., et al., 2020. Applications of geothermal organic Rankine Cycle for electricity production. J. Clean. Prod. 274, 122950.
Arslan, M., Yılmaz, C., 2022. Thermodynamic optimization and thermoeconomic evaluation of Afyon biogas plant assisted by organic rankine cycle for waste heat recovery. Energy 248, 123487.
Atelge, M.R., Senol, H., Djaafri, M., Hansu, T.A., Krisa, D., Atabani, A., et al., 2021. A Critical Overview of the state-of-the-art methods for biogas purification and utilization processes. Sustainability 13 (20), 11515.
Athari, H., Kiasatmanesh, F., Haghghi, M.A., Teymourzadeh, F., Yagoublou, H., Delpisheh, M., 2022. Investigation of an auxiliary option to meet local energy demand via an innovative small-scale geothermal-driven system; a seasonal analysis. J. Build. Eng. 50, 103902.
Azariyan, H., Vajdi, M., Takleh, H.R., 2021. Assessment of a high-performance geothermal-based multigeneration system for production of power, cooling, and hydrogen: thermodynamic and exergoeconomic evaluation. Energy Convers. Manag. 236, 113970.
Baghernejad, A., Yaghoubi, M., Jafarpur, K., 2016. Exergoeconomic comparison of three novel trigeneration systems using SOFC, biomass and solar energies. Appl. Therm. Eng. 104, 534–555.
Bamisile, O., Huang, Q., Anane, P.O., Dagbasi, M., 2019. Performance analyses of a renewable energy powered system for trigeneration. Sustainability 11 (21), 6006.
Behzadi, A., Arabkoohsar, A., Gholamian, E., 2020. Multi-criteria optimization of a biomass-fired proton exchange membrane fuel cell integrated with organic rankine cycle/thermoelectric generator using different gasification agents. Energy 201, 117640.
Bellos, E., Tzivanidis, C., 2021. Parametric analysis of a solar-driven trigeneration system with an organic Rankine cycle and a vapor compression cycle. Energy Built Environ. 2 (3), 278–289.
Cao, Y., Mohamed, A.M., Dahari, M., Delpisheh, M., Haghghi, M.A., 2020. Performance enhancement and multi-objective optimization of a solar-driven setup with storage process using an innovative modification. J. Energy Storage 32, 101956.
Cao, Y., Dhahad, H.A., Sun, Y.L., Haghghi, M.A., Delpisheh, M., Athari, H., Farouk, N., 2021a. The role of input gas species to the cathode in the oxygen-ion conducting and proton conducting solid oxide fuel cells and their applications: comparative 4E analysis. Int. J. Hydrogen Energy 46 (37), 19569–19589.
Cao, Y., Dhahad, H.A., Parikhani, T., Anqi, A.E., Mohamed, A.M., 2021b. Thermo-economic evaluation of a combined Kalina cycle and humidification-dehumidification (HDH) desalination system integrated with thermoelectric generator and solar pond. Int. J. Heat Mass Tran. 168, 120844.
Cao, Y., Dhahad, H.A., Rajhi, A.A., Alamri, S., Anqi, A.E., El-Shafay, A.S., 2022. Combined heat and power system based on a proton conducting SOFC and a supercritical CO2 Brayton cycle triggered by biomass gasification. Int. J. Hydrogen Energy 47 (8), 5439–5452.
Cavalcanti, E.J.C., 2017. Exergoeconomic and exergoenvironmental analyses of an integrated solar combined cycle system. Renew. Sustain. Energy Rev. 67, 507–519.
Chahartaghi, M., Sheykhi, M., 2018. Thermal modeling of a trigeneration system based on beta-type Stirling engine for reductions of fuel consumption and pollutant emission. J. Clean. Prod. 205, 145–162.
Chen, W., Huang, Z., Chua, K.J., 2022. Sustainable energy recovery from thermal processes: a review. Energy, Sustainability and Society 12 (1), 1–25.
Cheng, Z., Guo, Z., Fu, P., Yang, J., Wang, Q., 2021. New insights into the effects of methane and oxygen on heat/mass transfer in reactive porous media. Int. Commun. Heat Mass Tran. 129, 105652 https://doi.org/10.1016/j.icheatmasstransfer.2021.105652.
Cheng, F., Li, J., Zhou, L., Lin, G., 2023. Fragility analysis of nuclear power plant structure under real and spectrum-compatible seismic waves considering soil-structure interaction effect. Eng. Struct. 280, 115684.
Chicco, G., Mancarella, P., 2008a. Assessment of the greenhouse gas emissions from cogeneration and trigeneration systems. Part I: models and indicators. Energy 33 (3), 410–417.

Chicco, G., Mancarella, P., 2008b. Assessment of the greenhouse gas emissions from cogeneration and trigeneration systems. Part I: models and indicators. Energy 33 (3), 410–417.

Chitgar, N., Hemmati, A., Sadrzadeh, M., 2023. A comparative performance analysis, working fluid selection, and machine learning optimization of ORC systems driven by geothermal energy. Energy Convers. Manag. 286, 117072.

Dai, Y., Wang, J., Gao, L., 2009. Parametric optimization and comparative study of organic Rankine cycle (ORC) for low grade waste heat recovery. Energy Convers. Manag. 50 (3), 576–582.

Dincer, I., Rosen, M.A., Ahmadi, P., 2017. Optimization of Energy Systems. John Wiley and Sons.

dos Santos, R.O., de Sousa Santos, L., Prata, D.M., 2018. Simulation and optimization of a methanol synthesis process from different biogas sources. J. Clean. Prod. 186, 821–830.

Elsayed, M.L., Alharbi, S., Chow, L.C., 2021. Utilization of waste heat from a commercial GT for freshwater production, cooling and additional power: exergoeconomic analysis and optimization. Desalination 513, 115127.

Erixno, O., Abd Rahim, N., Ramadhani, F., Adzman, N.N., 2022. Energy management of renewable energy-based combined heat and power systems: a review. Sustain. Energy Technol. Assessments 51, 101944.

Fang, Z., Shang, L., Pan, Z., Yao, X., Ma, G., Zhang, Z., 2021. Exergoeconomic analysis and optimization of a combined cooling, heating and power system based on organic Rankine and Kalina cycles using liquified natural gas cold energy. Energy Convers. Manag. 238, 114148.

Fang, Y., Wang, H., Fang, P., Liang, B., Zheng, K., Sun, Q., Wang, A., 2023. Life cycle assessment of integrated bioelectrochemical-constructed wetland system: environmental sustainability and economic feasibility evaluation. Resour. Conserv. Recycl. 189, 106740 https://doi.org/10.1016/j.resconrec.2022.106740.

Ghorbani, B., Hamedi, M.H., Amidpour, M., Shirmohammadi, R., 2017. Implementing absorption refrigeration cycle in lieu of DMR and C3MR cycles in the integrated NGL, LNG and NRU unit. Int. J. Refrig. 77, 20–38.

Ghorbani, B., Mahyari, K.B., Mehrpooya, M., Hamedi, M.H., 2020. Introducing a hybrid renewable energy system for production of power and fresh water using parabolic trough solar collectors and LNG cold energy recovery. Renew. Energy 148, 1227–1243.

Goswami, D.Y. (Ed.), 2004. The CRC Handbook of Mechanical Engineering. CRC press.

Gu, H., Liu, J., Zhou, X., Wu, Q., Liu, Y., Yu, S., et al., 2023. Modelling of a novel electricity and methanol co-generation using heat recovery and CO2 capture: comprehensive thermodynamic, economic, and environmental analyses. Energy 278, 127481.

Guedri, K., Singh, P., Riaz, F., Inayat, A., Shah, N.A., Fadhl, B.M., Makhdoum, B.M., Arsalanloo, A., 2023. Solidification acceleration of phase change material in a horizontal latent heat thermal energy storage system by using spiral fins. Case Stud. Thermal Eng. 48, 103157. https://doi.org/10.1016/j.csite.2023.103157.

Haghghi, M.A., Hasanzadeh, A., Nadimi, E., Rosato, A., Athari, H., 2023. An intelligent thermodynamic/economic approach based on artificial neural network combined with MOGWO algorithm to study a novel polygeneration scheme using a modified dual-flash geothermal cycle. Process Saf. Environ. Protect. 173, 859–880.

Hai, T., Lin, H., Albdeiri, M.S., Alsenani, T.R., Elattar, S., Abed, A.M., Tian, R., 2023. A novel trigeneration model using landfill gas upgrading process and waste heat recovery: application of methanol, desalinated water, and oxygen production. J. Clean. Prod. 393, 136224.

Han, Y., Li, H., Liu, J., Xie, N., Jia, M., Sun, Y., Wang, S., 2023. Life cycle carbon emissions from road infrastructure in China: a region-level analysis. Transport. Res. Transport Environ. 115, 103581.

Hashemian, N., Noorpoor, A., 2019. Assessment and multi-criteria optimization of a solar and biomass-based multi-generation system: thermodynamic, exergoeconomic and exergoenvironmental aspects. Energy Convers. Manag. 195, 788–797.

He, J., Han, N., Xia, M., Sun, T., Ghaebi, H., 2023. Multi-objective optimization and exergoeconomic analysis of a multi-generation system based on biogas-steam reforming. Int. J. Hydrogen Energy 48 (55), 21161–21175.

Holagh, S.G., Haghghi, M.A., Mohammadi, Z., Chitsaz, A., 2020. Exergoeconomic and environmental investigation of an innovative poly-generation plant driven by a solid oxide fuel cell for production of electricity, cooling, desalinated water, and hydrogen. Int. J. Energy Res. 44 (13), 10126–10154.

Horlock, J.H., 1987. Combined Heat and Power.

Jalili, M., Ghasempour, R., Ahmadi, M.H., Chitsaz, A., Holagh, S.G., 2022. An integrated CCHP system based on biomass and natural gas co-firing: exergetic and thermo-economic assessments in the framework of energy nexus. Energy Nexus 5, 100016.

Ji-chao, Y., Sobhani, B., 2021. Integration of biomass gasification with a supercritical CO2 and Kalina cycles in a combined heating and power system: a thermodynamic and exergoeconomic analysis. Energy 222, 119980.

Jiang, J., Zhang, L., Wen, X., Valipour, E., Nojavan, S., 2022. Risk-based performance of power-to-gas storage technology integrated with energy hub system regarding downside risk constrained approach. Int. J. Hydrogen Energy 47 (93), 39429–39442.

Liu, L., Tang, Y., Liu, D., 2022a. Investigation of future low-carbon and zero-carbon fuels for marine engines from the view of thermal efficiency. Energy Rep. 8, 6150–6160. https://doi.org/10.1016/j.egyr.2022.04.058.

Liu, L., Wu, Y., Wang, Y., Wu, J., Fu, S., 2022b. Exploration of environmentally friendly marine power technology -ammonia/diesel stratified injection. J. Clean. Prod. 380, 135014 https://doi.org/10.1016/j.jclepro.2022.135014.

Liu, X., Zhao, H., Huang, Z., Shi, S., Guo, R., Ding, P., Xie, S., 2023. A comprehensive study of a novel multigeneration system using a combined power plant based on geothermal energy and oxyfuel combustion. J. Clean. Prod. 408, 137098.

Luján, J.M., Serrano, J.R., Dolz, V., Sánchez, J., 2012. Model of the expansion process for R245fa in an organic rankine cycle (ORC). Appl. Therm. Eng. 40, 248–257.

Mahmoudan, A., Esmaeilion, F., Hoseinzadeh, S., Soltani, M., Ahmadi, P., Rosen, M., 2022. A geothermal and solar-based multigeneration system integrated with a TEG unit: development, 3E analyses, and multi-objective optimization. Appl. Energy 308, 118399.

Mehrpooya, M., Sayyad, S., Zonouz, M.J., 2017. Energy, exergy and sensitivity analyses of a hybrid combined cooling, heating and power (CCHP) plant with molten carbonate fuel cell (MCFC) and Stirling engine. J. Clean. Prod. 148, 283–294.

Mofrad, K.G., Zandi, S., Salehi, G., 2023. Exergoeconomic and exergoenvironmental assessment of a geothermal-driven cogeneration system utilizing dual-pressure organic Rankine cycle and zeotropic mixtures. Energy Rep. 9, 5206–5223.

Mohammadi, A., Ashouri, M., Ahmadi, M.H., Bidi, M., Sadeghzadeh, M., Ming, T., 2018. Thermoeconomic analysis and multiobjective optimization of a combined gas turbine, steam, and organic Rankine cycle. Energy Sci. Eng. 6 (5), 506–522.

Mohammadi, M., Mahmoudan, A., Nojedehi, P., Hoseinzadeh, S., Fathali, M., Garcia, D. A., 2023. Thermo-economic assessment and optimization of a multigeneration system powered by geothermal and solar energy. Appl. Therm. Eng. 230, 120656.

Mores, P.L., Godoy, E., Mussati, S.F., Scenna, N.J., 2014. A NGCC power plant with a CO2 post-combustion capture option. Optimal economics for different generation/capture goals. Chem. Eng. Res. Des. 92 (7), 1329–1353.

Nami, H., Mahmoudi, S.M.S., Nemati, A., 2017. Exergy, economic and environmental impact assessment and optimization of a novel cogeneration system including a gas turbine, a supercritical CO2 and an organic Rankine cycle (GT-HRSG/SCO2). Appl. Therm. Eng. 110, 1315–1330.

Ogorure, O.J., Oko, C.O.C., Diemuodeke, E.O., Owebor, K., 2018. Energy, exergy, environmental and economic analysis of an agricultural waste-to-energy integrated multigeneration thermal power plant. Energy Convers. Manag. 171, 222–240.

Peng, D.Y., Robinson, D.B., 1976. A new two-constant equation of state. Ind. Eng. Chem. Fundam. 15 (1), 59–64.

Sadat, S.M.S., Ghaebi, H., Lavasani, A.M., 2020. 4E analyses of an innovative polygeneration system based on SOFC. Renew. Energy 156, 986–1007.

Sadeghi, M., Mehr, A.S., Zar, M., Santarelli, M., 2018. Multi-objective optimization of a novel syngas fed SOFC power plant using a downdraft gasifier. Energy 148, 16–31.

Safari, F., Dincer, I., 2019. Development and analysis of a novel biomass-based integrated system for multigeneration with hydrogen production. Int. J. Hydrogen Energy 44 (7), 3511–3526.

Salimi, M., Hosseinpour, M., Mansouri, S., Borhani, T.N., 2022. Environmental aspects of the combined cooling, heating, and power (CCHP) systems: a review. Processes 10 (4), 711.

Sarcheshmehpoor, M., 2019. Evaluation of a Gas Refinery Using Exergy-Based Methods. Technische Universitaet Berlin, Germany.

Sezer, N., Koç, M., 2019. Development and performance assessment of a new integrated solar, wind, and osmotic power system for multigeneration, based on thermodynamic principles. Energy Convers. Manag. 188, 94–111.

Siddiqui, O., Dincer, I., 2021. Sustainable utilization of agricultural bio-waste for multigeneration of electricity, heating, cooling and freshwater. J. Clean. Prod. 319, 128540.

Tian, C., Su, C., Yang, C., Wei, X., Pang, P., Xu, J., 2023. Exergetic and economic evaluation of a novel integrated system for cogeneration of power and freshwater using waste heat recovery of natural gas combined cycle. Energy 264, 126227.

Tzivanidis, C., Bellos, E., Antonopoulos, K.A., 2016. Energetic and financial investigation of a stand-alone solar-thermal Organic Rankine Cycle power plant. Energy Convers. Manag. 126, 421–433.

Wang, B., Gupta, R., Bei, L., Wan, Q., Sun, L., 2023. A review on gasification of municipal solid waste (MSW): syngas production, tar formation, mineral transformation and industrial challenges. Int. J. Hydrogen Energy 48 (69), 26676–26706.

Wang, Y., Abed, A.M., Kumar Singh, P., Tag-Eldin, E., Arsalanloo, A., 2022. Multi-Stage Optimization of LHTESS by utilization of Y-shaped Fin in a rectangular enclosure. Case Stud. Thermal Eng. 38, 102348. https://doi.org/10.1016/j.csite.2022.102348.

Wei, H., Su, C., Dai, J., Albdeiri, M.S., Alsenani, T.R., Elattar, S., et al., 2023. Towards a sustainable, and economic production future: proposing a new process for methanol production based on renewable hydrogen. J. Clean. Prod. 389, 135976.

Xiao, Y., Wu, S., Xia, H., Zhang, J., Ding, L., Bao, X., et al., 2023. Simulation of and multi-aspect study of a novel trigeneration process for crude helium, liquefied natural gas, and methanol production; operation improvement and emission reduction. Fuel 347, 128402.

Xu, Z., Li, X., Li, J., Xue, Y., Jiang, S., Liu, L., et al., 2022. Characteristics of source rocks and genetic origins of natural gas in deep formations, gudian depression, songliao basin, NE China. ACS Earth Space Chem. 6 (7), 1750–1771. https://doi.org/10.1021/acsearthspacechem.2c00065.

Xue, X., Li, J., Liu, J., Wu, Y., Chen, H., Xu, G., Liu, T., 2022. Performance evaluation of a conceptual compressed air energy storage system coupled with a biomass integrated gasification combined cycle. Energy 247, 123442.

Yu, D., Guo, J., Meng, J., Sun, T., 2023. Biofuel production by hydro-thermal liquefaction of municipal solid waste: process characterization and optimization. Chemosphere 328, 138606.

Zhang, Q., Zhang, N., Zhu, S., Heydarian, D., 2023. Thermodynamic simulation and optimization of natural gas liquefaction cycle based on the common structure of organic rankine cycle. Energy 264, 126134.

Zhao, J., Zhang, Q., Hao, W., Su, Q., 2023. Chemical absorption-based biogas upgrading process integrated with a novel poly-generation system: application of Aspen HYSYS simulation and 4E study. Process Saf. Environ. Protect. 174, 1023–1043.